Electrokinetic Properties of Electrolyte Mixtures

Understanding the consequences of adding monovalent electrolyte to divalent solutions

by

Rintati Roza

in partial fulfillment of the requirements for the degree of

Master of Science
in Mechanical Engineering

at the Delft University of Technology,
to be defended publicly on Wednesday June 2, 2021 at 14:00.

Supervisors:	Dr. R. M. Hartkamp
	Ir. M. F. Döpke
Thesis committee:	Dr. R. M. Hartkamp
	Ir. M. F. Döpke
	Prof. dr. ir. J. T. Padding

An electronic version of this thesis is available at http://repository.tudelft.nl/.

Preface and acknowledgements

When I started my first year of my Aerospace Engineering bachelor, I had no clue that I would end up doing a thesis about solid-liquid interfaces. Nevertheless, the shift to the Energy and Process Technology master track at Mechanical Engineering is something I haven't once regretted and this work is the final step towards graduation. Doing a thesis during a global pandemic is obviously not all fun and games. The excitement of learning new things about a completely new discipline and acquiring new skills quickly alternated with the tough process of getting to know yourself when things go not as smoothly as planned.
I want to express my gratitude to my supervisors, Remco Hartkamp and Max Döpke, for their availability and help throughout this thesis. Thanks for the insightful discussions and involvement with my work. It is a pity that we couldn't have in-person meetings more often. Fenna, thank you for helping me starting my project and setting a good example for me, and also for your kind words after you graduated.
I also want to thank my rowing team for their daily support. Combining a thesis and rowing 12 hours a week is tough, but it also kept me sane and healthy. Thanks to Jos, Jan and Willem for their feedback throughout the process. Finally, I want to thank my parents, my boyfriend and best friends Amber and Lemin for helping me put everything in perspective whenever I needed it.

Rintati Roza
Delft, May 2021

Abstract

This thesis aims to find out whether electrokinetic transport of a calcium chloride solution can be controlled by adding sodium ions by performing molecular dynamics simulations. The idea that electrokinetic transport control is a possibility originates from research that found that charge inversion is reduced when monovalent ions are added to a multivalent solution. Consequently, flow reversal suppression is expected. Many mechanisms are known to contribute to charge inversion and ion competition, but it is unclear how they exactly relate to charge inversion reduction and flow reversal suppression.

This work aims to replicate charge inversion reduction and flow reversal suppression in a system with an amorphous silica interface for mixed electrolytes with calcium, sodium and chloride. To allow insight into the structural behaviour of the electrical double layer and the electrokinetic properties for varying concentrations, molecular dynamics simulations are used.

No variation in charge inversion and flow reversal reduction was found for the simulated concentrations. However, the adsorption behaviour of ions in the electrical double layer changed due to ion competition between sodium and calcium, where sodium outcompetes calcium for inner sphere surface complex adsorption. This work also shows that the electroosmotic flow behaviour for mixtures is sensitive to the dynamic adsorption behaviour of ions, emphasizing the importance of correctly tuned force field parameters between surface and ions.

Contents

List of Figures

List of Tables

List of Symbols

Latin symbols

a	Adsorption type	
c	Concentration	[mole/L]
c_0	Critical concentration	[mole/L]
d	Distance to the nearest wall atom	[nm]
D	Transport diffusion coefficient	[nm]
e	Electron charge	[C]
E	Electric field strength	[V/nm]
F	Force	[kcal/(mole.Å)]
f	Scaling factor	[-]
I	Ionic strength	[mole/L]
I_{str}	Streaming current	[A]
i	Ion species or particle	
K_1	Spring stiffness for bonds	[kcal/mole/Å^2]
K_2	Spring stiffness for angles	[kcal/mole]
k_b	Boltzmann constant	[J/K]
M	Mole/L	
m	Mass	[grams/mole]
N	Amount of samples	[-]
q_e	Charge density	[C/m^2]
r	Position	[Å]
S_{str}	Streaming conductance	[A/bar]
T	Temperature	[K]
t	Time	[s]
u	Velocity	[m/s]
U	Potential energy	[kcal/mole]
z	Distance to the wall	[nm]
Z	Valency	[-]

Greek symbols

ϵ	Permittivity	[F/m]
ϵ_{ij}	Lennard-Jones energy parameter	[kcal/mol]
ϵ_0	Vacuum permittivity	[F/m]
ϵ_r	Relative permittivity	[-]
η	Viscocity	[Pa.s]
Γ	Screening	[C/m^2]
μ	mean	
ϕ	Electrokinetic potential	[V]
ρ_n	Number density	[nm^{-3}]
σ	standard deviation	
σ_{ij}	Lennard-Jones distance parameter	[Å]
σ_0	Bare surface charge	[C]
θ	Angle	[-]
ζ	Zeta potential	[V]

List of Abbreviations

AFM	Atomic force microscopy
CI	Charge inversion
CoSep	Cobalt(III)sepulchrate
DS	Diffuse species
EDL	Electrical double layer
EOF	Electroosmotic flow
FI	Free ions
FR	Flow reversal
GCSG	Gouy-Chapman-Stern-Grahame
HS	Helmholtz-Smoluchowski
IFF	Interface force field
IHP	Inner Helmholtz plane
ISSC	Inner sphere surface complex
LAMMPS	Large-scale atomic/molecular massively parallel simulator
LJ	Lennard-Jones
MD	Molecular dynamics
NVE	Microcanonical ensemble
NVT	Canonical ensemble
NS	Navier-Stokes
OHP	Outer Helmholtz plane
OSSC	Outer sphere surface complex
PB	Poisson-Boltzmann
PBC	Periodic boundary condition
RAXR	Anomalous X-ray reflectivity
SC	Streaming current
SCL	Strongly correlated liquid
SCM	Surface complexation model
SFA	Surface force apparatus
XPS	X-ray photoelectron spectroscopy

1 Introduction

One of the first things we learn about science while growing up is the importance of water on life on earth. More than 70% of the earth is covered in water, and on average 60% of the human body consists of water [2, 3]. On a nanoscale level, most of these natural systems do not only consist of water, but also mixtures of ion species can be found. Many nanofluidic applications are being developed, for example, for water desalination [4]. However, the focus of fundamental studies researching nanofluidics has been mostly on aqueous electrolytes composed of a single salt species. This work researches the electrokinetic properties of aqueous electrolyte mixtures confined by amorphous silica by performing molecular dynamics experiments. The electrokinetic behaviour is established by using an electrical field. This chapter gives an introduction to the rest of the report, including an explanation of the relevance of the presented research. First the background information on the topic is explained in section 1.1, followed by the identification of the research gap in section 1.2. Then the research questions are presented in section 1.3. Finally, the outline of the work is given in section 1.4.

1.1. Background Information

Nanofluidics is the field where transport of liquids confined by nanostructures (1-100 nm) is investigated. Many biological phenomena, such as DNA transport and drug delivery, take place at this length scale. Research into nanofluidic devices has become increasingly interesting due to their possible applications. Power harvesting, DNA and RNA experiments in biotechnology and desalination of water are a few examples [4–6]. To establish transport in nanofluidic devices, electroosmotic flow can be used. Electroosmotic flow is fully determined by the electrical double layer. The electrical double layer and electroosmotic flow are two definitions that are crucial to understanding the research in this thesis. They are briefly explained below.

The electrical double layer

When an aqueous ionic solution and solid are brought in contact, the solid will become charged, and the ions in the liquid form a layer on the solid to compensate for this charge. Together, the charged wall and the compensating ions are called the electrical double layer (EDL). This thesis uses amorphous silica surface material. Silica is one of the earth's most abundant elements. It is easily produced and manipulated, making it a suitable material for

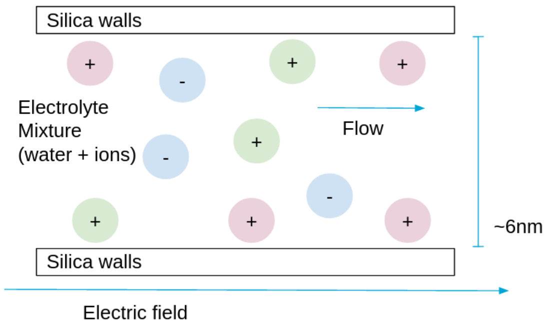

Figure 1.1: A schematic overview of the system in this work.

nanofluidic devices [7]. For example, it has been used in a study investigating nano transistors that can be used as a blood diagnostic tool [8]. When amorphous silica is submerged in a liquid with a neutral to high pH, the surface becomes negatively charged. Anions are therefore repelled from the surface, whereas cations are attracted to the surface, compensating for the surface charge. Together, the charged surface and the ions close to the wall form an electrical double layer, in which the net charge is zero. The EDL is important for nanofluidic systems, because the system size is the same order of magnitude as the size of the EDL (large surface-to-volume ratio). In systems with a high ionic strength, charge inversion (CI) might occur, which means that the cations in the EDL overcompensate for the bare surface charge. For more information about the EDL, refer to section 2.1.

Electroosomotic flow

Transport through a nanochannel can be established with various methods, for example by applying a pressure difference, a temperature difference or an electric field. The coupled transport of fluid and movement of charges that follows leads to different electrokinetic phenomena. These phenomena have great importance in the applications of nanofluidic devices, such as blue energy harvesting, enhanced oil recovery, chemical separation and DNA sensing [4, 9–11]. It also has its applications in biotechnology [8]. This research will consider the transport through a system that is driven by an electric field. If an electric field is applied to the system, the charged ions will move, and the water will be dragged along. This transport of water is called electroosmotic flow (EOF). The direction of this flow in the channel is entirely determined by the EDL because the net charge is neutral in the bulk. For a negatively charged surface, the EDL generally contains more cations than anions. This means that the net flow is expected to move in the positive direction. When the flow moves into the negative direction instead, which might happen when CI occurs, this is called flow reversal (FR). More information about electrokinetic phenomena can be found in section 2.2.

Figure 1.1 shows a simplified image of the system in this research, which uses an electric field to establish transport of fluid in the channel. The fluid exists of an aqueous mixture of monovalent and divalent electrolyte, and the solid walls consist of amorphous silica.

1.2. Literature Review

Currently, the electrokinetic transport properties of electrolyte mixtures are barely being investigated. At the same time, almost all natural electrolytes exist of such mixtures. One of the key studies investigating charge inversion for electrolyte mixtures has been the research done by Van Der Heyden *et al.* [1]. They used streaming currents as their method to investigate charge inversion. A pressure difference is applied, which leads to a streaming current due to the imbalance of charges in the EDL. The streaming conductance (S_{str}) is the streaming current per pressure unit. With this method, ionic strengths up to 1 mol/L (M) can be accurately considered, which is needed to access the regime in which charge inversion occurs.

The system used in the study by Van der Heyden *et al.* had an amorphous silica wall and the measurements were performed at a near-neutral pH of 7.5. They did the experiment for divalent magnesium chloride ($MgCl_2$) and calcium chloride ($CaCl_2$), trivalent cobalt(III)sepulchrate chloride ($CoSepCl_3$), and mixtures of $CoSepCl_3$ and monovalent potassium chloride (KCl) solutions. Charge inversion was found for divalent and trivalent electrolytes, starting from a certain ionic strength. The critical concentration (c_0) is the concentration at which charge inversion starts occurring. For CoSep, the critical concentration is $3.3 \cdot 10^{-4}$ M. For $MgCl_2$ and $CaCl_2$, the critical concentration is around 0.4 M. The trend seems to be that charge inversion increases with increasing ionic strength.

Where most studies only consider the electrokinetic properties of single electrolytes, Van der Heyden *et al.* have also conducted the experiment for electrolyte mixtures. Adding monovalent KCl to trivalent $CoSepCl_3$ causes an ionic strength increase; thus the expectation is that charge inversion increases as well. However, the experiment showed that charge inversion decreases due to the addition of the monovalent salt, up to a certain point, after which it increases again. Consequently, flow reversal and flow reversals reduction are also expected. The result is schematically shown in figure 1.2.

This phenomenon was also found in studies that research colloidal electrophoresis [12–14]. They measured the electroosmotic mobility of a charged colloid. Because the particle's size is considerably larger than the width of the EDL, the system can be compared to a system with a flat surface on which an EDL forms. Mobility reversal of the colloid is similar to flow reversal of EOF. They found that for trivalent and other higher valency electrolytes, colloid mobility reversal is suppressed when lower valency ions are added.

A clear in-depth explanation for decrease of charge inversion is currently lacking. It is known that calcium uptake on a surface decreases when monovalent sodium chloride is added [15]. This can explain the CI reduction measured by Van Der Heyden, assuming that monovalent sodium ions replace the divalent calcium ions [16]. This also indicates that ion valency is not the only driving factor for ion adsorption onto the surface, since higher valency ions experience a higher attractive electrostatic force from the surface [17]. Understanding the ion competition in the EDL might be the key to explaining the decreasing CI when monovalent ions are added to a multivalent solution.

Molecular dynamics (MD) simulations can be used to study the phenomena in the EDL on an atomic scale without performing physical experiments. The movements of ions in the system can be directly analysed. Döpke *et al.* [18] studied the adsorption competition in a system of calcium chloride and sodium chloride. Calcium ions have a stronger hydration shell than sodium ions, due to their higher valency. They found that this hydration shell

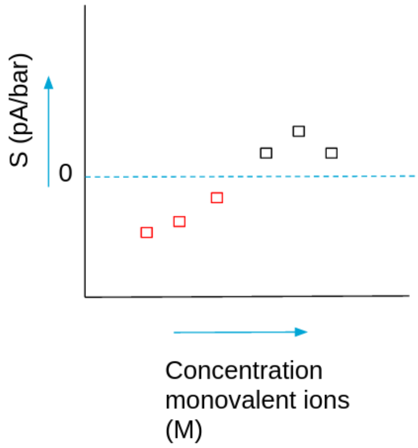

Figure 1.2: Schematic results for streaming conductance of a trivalent/monovalent mixture. The red squares below zero depict charge inversion, which disappears when the monovalent concentration increases.

might cause steric hindrances for calcium adsorption on rough surfaces like amorphous silica. This results in preferential adsorption of sodium on some spots on the surface.

Bourg and Sposito [19] have used MD simulations for calcium chloride and sodium chloride mixtures on a smectite surface, which has a regular structure. They found that formation of $CaCl^+$ ions occurs, which contributes to the occurrence of CI. Szymanek *et al.* [17] and Brugman *et al.* [20] both also found that inclusion of co-anion adsorption was needed to fit their surface complexation models on their data on ion adsorption in mixtures.

It is shown that charge inversion can be related to decreased mobility of the counterions in the EDL, which contributes to flow reversal [21, 22]. Although it is clear that charge inversion and flow reversal are related, it is not exactly known how. In section 2.4, a more in-depth overview of the current state of the art is described.

Although we have many indications of which mechanisms can cause charge inversion and contribute to ion competition, there has not been an MD study that aims to replicate the charge inversion suppression and flow reversal reduction in a system with amorphous silica. MD simulations can concurrently sample the structural and dynamic properties of a system, allowing insight into the ion competition in the EDL and how that translates to the EOF. If the EOF of multivalent electrolytes can be controlled by adding monovalent ions, the development of nanofluidic devices can be improved.

This thesis will use MD simulations to study a system consisting of calcium chloride and sodium chloride, applying an electric field to establish electroosmotic flow. The aim is to replicate the phenomenon of decreasing charge inversion and flow reversal upon increasing sodium chloride concentration. This is possible because the critical concentration for $CaCl_2$ was found to be 0.4 M, which is a concentration that can be accessed by MD simulations. With MD the adsorption in the EDL will be closely studied, providing insight into the charge inversion phenomenon. Also, the effect of adding monovalent ions on flow reversal and flow reversal reduction can be studied. This thesis also aims to give insight into the relation between the structural properties of the EDL and the electrokinetic properties of the system.

1.3. Research Questions

This thesis aims to determine how charge inversion and electrokinetic properties are affected by adding monovalent NaCl to a divalent $CaCl_2$ solution around the critical concentration. To research this, molecular dynamics simulations are used.

The hypothesis is:

> **Adding sodium ions to a calcium chloride solution leads to a decrease of charge inversion, which also reduces the flow reversal effect.**

Coupled to the following research question:

> **Can the transport of a calcium chloride solution be controlled by adding sodium chloride?**

If the answer to this question is yes, this would be a step forward towards designing nanofluidic applications suitable for electrolyte mixtures. This research question can be divided into the following subquestions:

- **How does adding sodium chloride to a calcium chloride mixture affect the charge inversion and the flow reversal?**

This research aims to replicate the decrease of charge inversion when monovalent ions are added to a multivalent solution.

- **How do different ion types adsorb at the surface?**

Competitive adsorption behaviour on the surface will affect the electrokinetic properties of the system. Therefore, it is important to see how the addition of monovalent electrolyte impacts the EDL.

- **How do electrokinetic properties relate to the EDL structure for mixed electrolytes?**

There is a link between charge inversion and flow reversal. This research aims to investigate how flow properties relate to the structural properties of the EDL for an electrolyte mixture.

1.4. Outline

This report consists of a theoretical background in chapter 2, giving all information needed to fully understand the research performed. It is followed by chapter 3, which explains the methodology of this thesis. It contains a detailed explanation of how Molecular Dynamics simulations work, and the steps followed to establish the results of the research. Chapter 4 contains the verification of the simulations and post-processing to confirm that they are carried out properly. In chapter 5 the results are shown and discussed in the context of existing literature. Finally, the conclusion and recommendations can be found in chapter 6.

2

Theoretical Background

This chapter will provide the necessary background knowledge to understand the work carried out in this work. First, several aspects of the electrical double layer (EDL) are explained in section 2.1. Second, the electrokinetics that are involved with this thesis are described in section 2.2. In section 2.3, analytical models and experimental and computational methods that are commonly used to characterize and measure the EDL are explained. Finally, the state of the art is illustrated in section 2.4.

2.1. The Electrical Double Layer

A closer look at the electrical double layer is needed to explain the macroscopic properties of the system. This section describes the models used for interpretation of the EDL, charge inversion (CI), the properties of amorphous silica and the description of different ions in the solution.

2.1.1. Interpretation of the EDL

The most basic description of the electrical double layer defines two charged layers parallel to the surface. The first layer coincides with the surface, containing the bare surface charge and the ions that are chemically adsorbed onto the surface. The second layer contains the other ions that are adsorbed in the liquid due to Coulombic interactions. The net charge of the electrical double layer is zero: the two layers compensate for each other.

There are different models that interpret the EDL further. An example is the Gouy-Chapman-Stern-Grahame (GCSG) model. It defines a Stern layer and the diffuse layer. In the Stern layer, it is assumed that the ions are immobile due to their adsorption on the surface. Within the Stern layer, the inner Helmholtz plane (IHP) and the outer Helmholtz plane (OHP) are defined. The IHP coincides with the nuclei of the ions adsorbed directly to the surface, whereas the OHP coincides with the center of the ions adsorbed with a water molecule between the wall and the ion. The second layer is the diffuse layer, whose width scales linearly with the Debye length λ_d [23]. The Debye length is defined as the length at which it is assumed that ions do not interact anymore. λ_d scales with the inverse of the salt concentration, so the higher the concentration, the more narrow the EDL. The wall interface, Stern layer and the diffuse layer form the EDL together. The middle of the channel is called the bulk. This GCSG-model or similar descriptions are at the base of the conventional analytical models to describe the EDL. Figure 2.4 shows a schematic of the GSGC-model.

2.1.2. Charge Inversion

This section describes charge inversion by means of the screening function. The screening function describes to what extent the surface charge is compensated for by the interfacial ions in the EDL. Equation 2.1 shows its definition.

$$\Gamma(z) = \sigma_0 + \int_{min(z)}^{z} \sum_i \rho_{n,i}(z) Z_i dz \tag{2.1}$$

σ_0 represents the bare surface charge, z is the distance to the wall and $\rho_{n,i}$ and Z_i are the number density and valency per ion species. In figure 2.1, the blue line represents what the screening function classically should look like for a negatively charged surface. The line starts at a negative value, which is the bare surface charge. Throughout the EDL a decrease in absolute charge is visible, due to the excess of counterions, until the net charge ultimately becomes zero in the bulk.

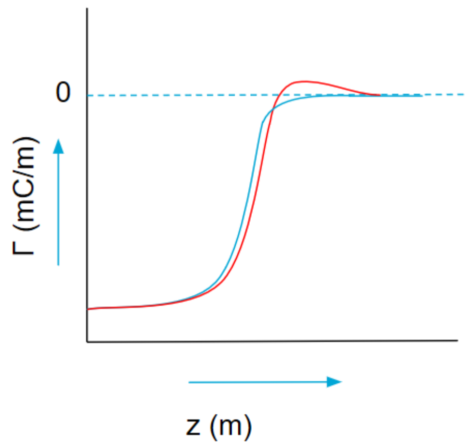

Figure 2.1: The screening function. The blue line depicts regular screening of a surface, the red line shows charge inversion, also called overscreening.

The ionic strength (I) of an electrolyte influences the screening in the EDL. The ionic strength is described in equation 2.2. It is a combination of the valency (Z_i) of the ions present and their concentration (c_i).

$$I = 0.5 \sum_i c_i Z_i^2 \tag{2.2}$$

For electrolytes with a high ionic strength, the situation might deviate from the blue line in figure 2.1. The interfacial ions can overcompensate for the bare surface charge. This phenomenon is called charge inversion, or overscreening. It is represented by the red line in figure 2.1.

2.1.3. The Solid Part of the EDL: Amorphous Silica

This thesis will use an amorphous silica interface. This section explains what amorphous silica is, and which properties influence the adsorption behaviour.

Structural properties of amorphous silica

Amorphous silica consists of a random network of silicon dioxide (SiO_2). Each silicon atom is bonded to four oxygen atoms and each oxygen atom is bonded to two silicon atoms. At the surface, not every oxygen atom has two silicon neighbours. These dangling oxygen atoms form a bond with a hydrogen atom instead, forming silanol groups (SiOH). They are also called surface groups.

Due to the patternless structure of the silica, the surface groups may vary in height. It can vary up to multiple nanometers, which is in the same order of magnitude as the Debye length for higher concentrations [24]. Consequently, it is not possible to define a clear, straight IHP or OHP through the center of the ions [25]. This is visualised in figure 2.2. Therefore, the commonly used GSCG-model of the EDL is not accurate for amorphous silica, whereas for other surfaces that are less rough and unstructured, for example smectite, the different planes can indeed be distinguished [19, 26].

Figure 2.2: A visualisation of how the surface roughness prevents the IHP to be defined in straight planes, as is done in the GSGC-model.

Deprotonation and protonation

The silanol groups can protonate or deprotonate according to reaction 2.3 and 2.4 respectively. It has been shown that protonation (equation 2.3) of the silicon surface groups does not occur in the normal pH-range (3-9) of experiments [27], which explains why the bare surface charge of silica in this work is negative.

$$\equiv SiOH + H^+ \Leftrightarrow \equiv SiOH_2^+ \tag{2.3}$$

$$\equiv SiOH \Leftrightarrow \equiv SiO^- + H^+ \tag{2.4}$$

Deprotonation of the silica surface shifts more to the right-hand side of equation 2.4 for an increasing pH-value [17, 28]. This results in an increasingly negative surface charge, as can be seen in figure 2.3. Similarly, the surface charge decreases for an increasing ionic concentration [17, 29].

2.1.4. The Liquid Part of the EDL: Classification of Ions

The ions in the electrolyte can be classified according to their adsorption behaviour. In this work, four different types are distinguished: Inner Sphere Surface Complexes (ISSC), Outer Sphere Surface Complexes (OSSC), Diffuse Species (DS) and Free Ions (FI). They can be seen in figure 2.4.

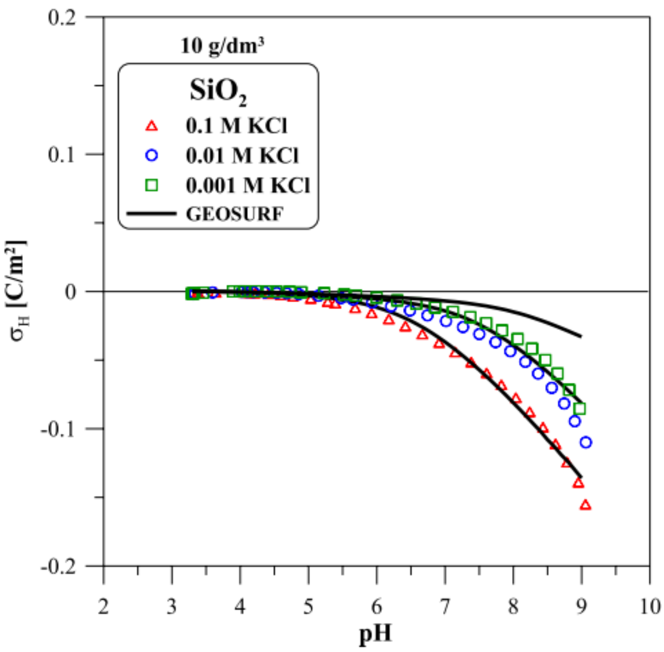

Figure 2.3: The surface charge decreases for increasing pH and increasing ionic concentration. Taken from Szymanek *et al.* [17].

ISSC's are directly connected to the surface and thus have a disrupted hydration shell and OSSC's are separated from the wall by one water molecule. ISSC and OSSC species are considered to be practically immobile. The diffuse species are still loosely associated to the wall, so they do not exhibit bulk flow behaviour. The free ions are not influenced by the wall.

A typical EDL model such as the GCSG-model assumes that all ISSC's lay within the inner Helmholtz plane, all OSSC's lay within the outer Helmholtz plane, all DS's lay in the diffuse layer and are free ions are in the bulk. In section 2.1.3, it is explained that this is not accurate for amorphous surfaces.

2.2. Electrokinetics

This work will investigate the electrokinetic properties of a system with electroosmotic flow. This section first describes the three most relevant electrokinetic phenomena for this thesis. Then, flow reversal (FR) is explained.

2.2.1. Electrokinetic Phenomena

Transport of fluid and charged particles in the fluid through a nanochannel can be realised by applying a gradient, for example, a pressure difference, a temperature difference or an electric field. The origin of electrokinetic effects lies in the coupling between fluid motion and the motion of charged particles. This section describes streaming currents, electroosmotic flow and electrophoresis. Streaming currents are driven by pressure and the latter two by an electric field. The impact of the EDL on these three electrokinetic phenomena is very similar, which makes research into one of the phenomena also applicable to the other two.

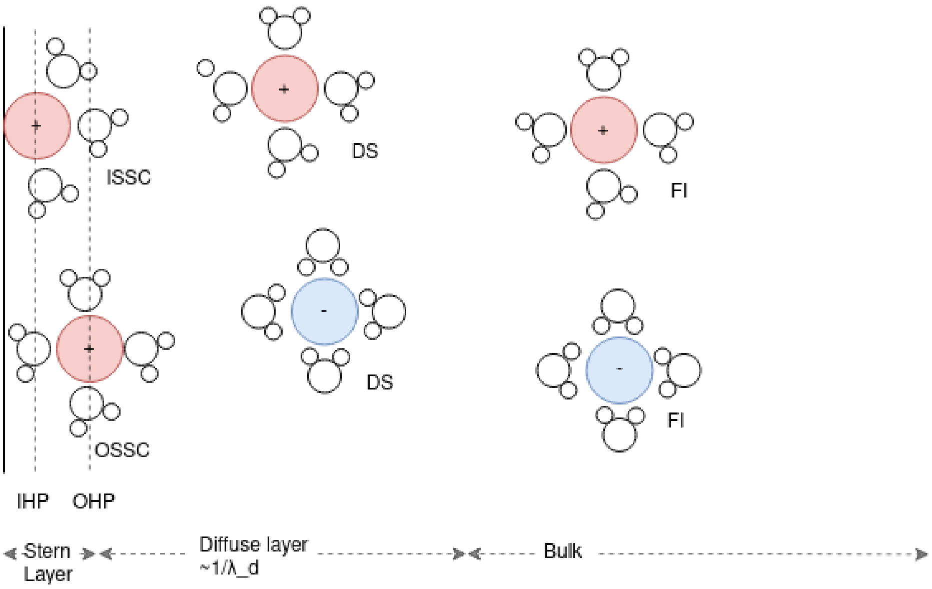

Figure 2.4: On the top: classification of ions into ISSC (Inner Sphere Surface Complex), OSSC (Outer Sphere Surface Complex), DS (Diffuse Species) and FI (Free Ions). On the bottom: the layers that define the system according to the GCSC-model.

Streaming currents

If a pressure difference is applied to a confined electrolyte, the fluid will move as a Poiseuille (parabolic) flow, dragging the ions along in the same direction. Because of the imbalance of cations and anions in the EDL on the static solid surface, a current is generated along the channel. This is visualised in figure 2.5. The generated current is called the streaming current (I_{str}).

A positive streaming current means that there is an abundance of positive ions in the mobile part of the EDL. If charge inversion occurs, the adsorbed (immobile) positive ions overcompensate the surface charge, resulting in an abundance of negative ions moving through the EDL. This results in a negative streaming current. The streaming current per unit of applied pressure is called the streaming conductance (S_{str}).

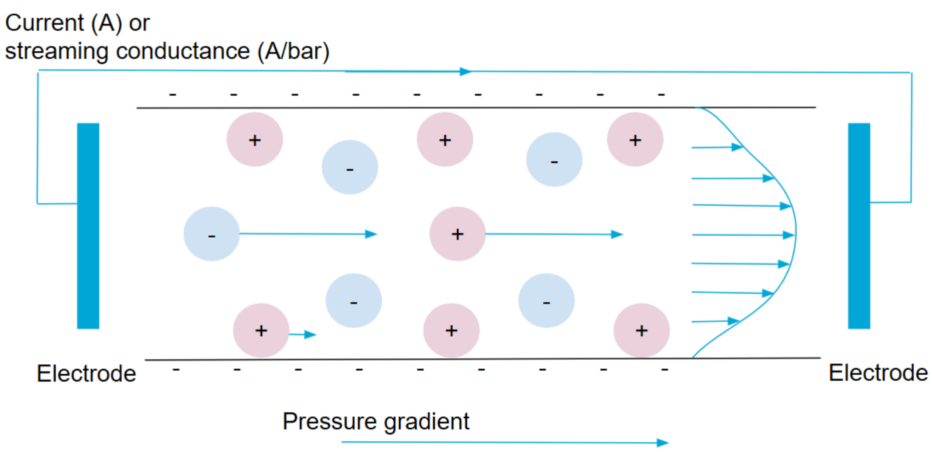

Figure 2.5: A schematic overview of streaming current.

Electroosmosis

If an electric field is applied to a confined electrolyte, the charged ions will move, and the water will be dragged along. The net charge in the bulk is zero, as the anions and the cations compensate for each other. The direction of this flow in the channel is therefore entirely determined by the EDL.

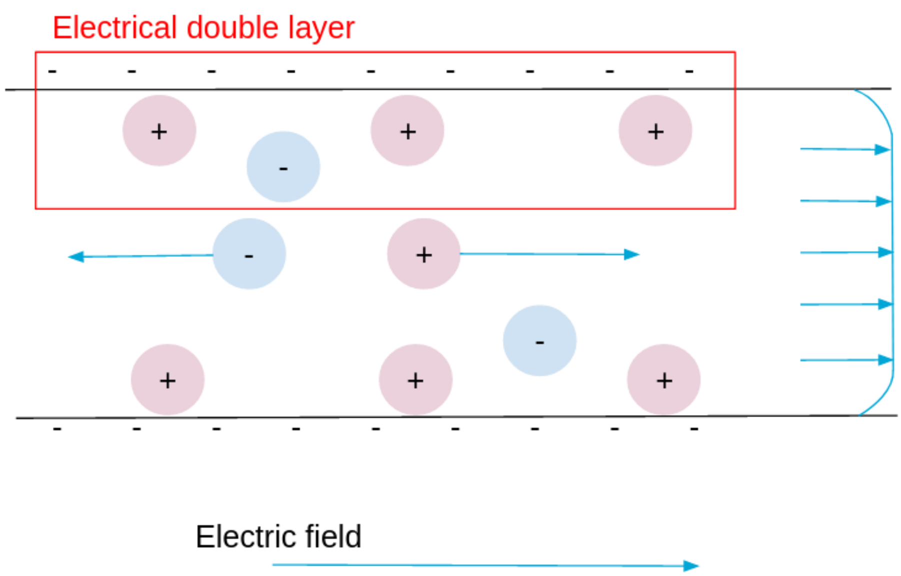

Figure 2.6: A schematic overview of electroosmotic flow.

For a negatively charged surface, the EDL generally contains more cations than anions. This means that the net flow is expected to move in the positive direction. This results in a plug flow velocity profile, which is constant in the bulk. The flow in the bulk is called the electroosmotic flow (EOF). Concluding, the EOF is independent of the channel width and is entirely determined by what happens in the EDL. A schematic of the system, the EDL and the velocity profile can be seen in figure 2.6.

Electrophoresis

If solid colloids are submerged into an aqueous ionic solution, the colloid surface will become charged and an EDL is formed. If an electric field is applied to such a system, the colloids will move depending on their surface charge and the screening by the EDL. The movement of the colloids is called electrophoretic mobility. Electrophoresis and electroosmosis are thus similar phenomena, but electrophoresis has a moving solid (colloids) and electroosmosis has a static solid (the wall).

2.2.2. Flow Reversal

Generally speaking, there is an abundance of counterions present in the EDL. The velocity profile that one would consequently expect for EOF (in a system with a negatively charged surface) has the shape of a plug flow as shown by the blue line in figure 2.7.

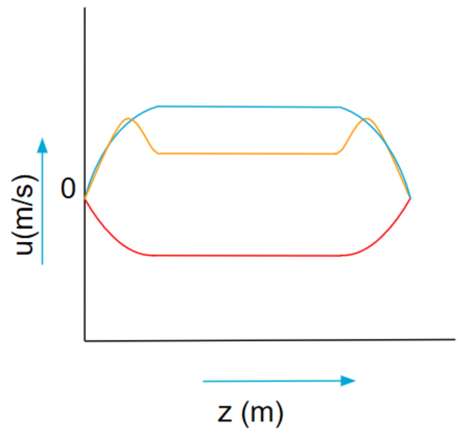

Figure 2.7: The velocity profile for EOF in a channel with a negatively charged surface. The blue line shows a regular plug flow profile, the red line shows flow reversal and the orange line shows a flow reversal tendency.

However, if the cations are strongly attracted to the wall, for example when CI occurs, they become partially immobilized. If they are immobilized to such an extent that the co-ions dominate the flow in the EDL, the flow direction of the fluid in the bulk reverses. This is called flow reversal (FR), represented by the red line in figure 2.7. The orange line shows a tendency towards FR. In electrophoresis, a similar phenomenon to FR can happen: If the counterions on the colloids become dominant to their mobility, the electrophoretic mobility flips sign.

2.3. Methods to Investigate the Electrical Double Layer

Various methods exist to investigate and represent the EDL. Generally, three large categories of methods are distinguished: analytical models, experiments and computational models. This section will discuss the relevant methods for investigating the EDL and its electrokinetic properties.

2.3.1. Analytical Models

This section describes the Poisson-Boltzmann equation, the Navier-Stokes equation and surface complexation models. These are commonly used analytical models that describe the structural and electrokinetic properties of the EDL.

The Poisson-Boltzmann equation

The Poisson-Boltzmann (PB) equation is the standard textbook description of the structural properties of the electrical double layer. The PB-equation and the Navier-Stokes equation (described in section 2.3.1) also referred to as continuum theory. The PB equation combines the Poisson equation of electrostatics and the Boltzmann distribution from statistical physics [30]. The diffuse layer can be accurately described by the Poisson-Boltzmann equation for dilute solutions. In figure 2.8, the shape of the electric potential and the predicted density profiles obtained by PB can be seen.

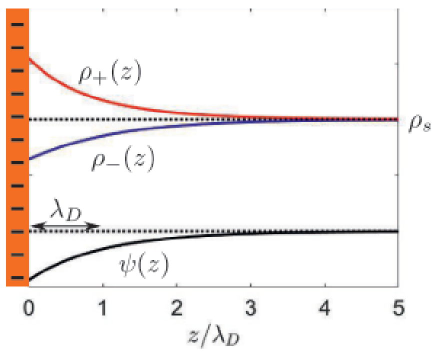

Figure 2.8: The negative and positive charge density profiles and the electric potential along the channel as predicted by Poisson-Boltzmann. Figure taken from Werkhoven [30].

The Poisson equation as shown in equation 2.10 relates the electric potential ϕ to the local charge density ρ_e. ϵ is the permittivity of the solvent, e is the electron charge, and z_i and ρ_i are the valency and number density of the ions.

$$\Delta^2\phi(\mathbf{r}) = -\frac{\rho_e(\mathbf{r})}{\epsilon} = \frac{e}{\epsilon}\sum Z_i\rho_{n,i}(\mathbf{r}) \tag{2.5}$$

The Poisson equation is often used by MD studies to relate their obtained structural profiles to the electric potential [25]. This work will also use the Poisson equation as described in section 3.3. To solve the Poisson equation, two boundary conditions are applied. The first one is a Dirichlet boundary condition for the bulk as described in 2.6. Because the net charge in the bulk is neutral, the electric potential goes to zero.

$$\phi(bulk) = 0 \tag{2.6}$$

The second boundary condition is applied at the surface. The surface has a set surface charge, which can be described using Gauss' law of electrostatics as shown in equation 2.7. Here, z_σ is the sign of the surface charge and σ is the surface charge density. Because it describes the derivative of the electric potential, this is a Neumann boundary condition.

$$\nabla\phi(r = wall) = -\frac{z_\sigma e\sigma_0}{\epsilon} \tag{2.7}$$

The nonlinear Poisson-Boltzmann equation is a combination of equation 2.10 and the Boltzmann distribution depicted by equation 2.8. The Boltzmann distribution is a probability density function describing the density profile of particles. It provides a second relation between the electric potential and the density profile. $\rho_{b,i}$ is the density in the bulk for ion type i, T is the temperature which is assumed to be a system constant, and k_b is the Boltzmann constant.

$$\rho_i(\mathbf{r}) = \rho_{b,i}e^{-z_i\frac{e}{k_bT}\phi(\mathbf{r})} \tag{2.8}$$

Within the PB-equation, many simplifications are made. For example, the ions are considered as point charges and the surface is considered as a flat surface where the charge is uniformly distributed. These simplifications lead to the inability of the PB-equation to predict charge inversion, which will be discussed in 2.4. Several theories have been put forward trying to refine the PB-model. Strongly Correlated Liquid theory (SCL) for example, is an adaptation of the Poisson-Boltzmann equation which assumes that the interaction between counterions on the surface is stronger than what is predicted by the Poisson-Boltzmann equation. According to SCL theory, the interfacial ions can form a strongly correlated liquid, which explains charge inversion.

Electrokinetic properties

The velocity profile can be modelled for a one-dimensional, steady state system with Navier-Stokes' (NS) equation for conservation of momentum, which is given by equation 2.9. Here, u is the velocity in the channel, ρ is the charge density, η is the viscosity of the solution, and E is the applied electric field.

$$\frac{\partial^2 u}{\partial z^2} = -\frac{\rho_e}{\eta}E \tag{2.9}$$

For experimental methods, it is useful to be able to couple the electric potential to the electroosmotic flow velocity. The shear plane is defined for that purpose. Remember that the classical definition of the Stern layer assumes that all adsorbed ions are completely immobile. Thus, there must be a plane (close to) the OHP where the flow velocity is zero. This is called the shear plane. The electric potential at the location of the shear plane is called the zeta potential (ζ).

The Poisson equation (2.10) relates the electrokinetic profile Ψ to the local charge density in the channel. It is also part of the PB-equation. Here, ϵ_r is the relative permittivitty of the solvent and ϵ_0 the vacuum permittivitty .

$$\nabla^2\phi(\mathbf{r}) = -\frac{\rho_e(\mathbf{r})}{\epsilon_r\epsilon_0} \tag{2.10}$$

Combining the Poisson equation, the Navier-Stokes equation (2.9) and boundary conditions 2.11 and 2.12, a new relation can be obtained. This is the Helmholtz-Smoluchowski (HS) equation, shown in equation 2.13.

$$\psi(z_{bulk}) = 0 \tag{2.11}$$

$$\psi(z_{shear}) = \zeta \tag{2.12}$$

$$u_{eof} = -\frac{\epsilon_0\epsilon_r\zeta}{\eta}E \tag{2.13}$$

Surface complexation modelling

Surface Complexation Modelling (SCM) is a different approach that focuses on the formation of ions into different surface complexes. With this method, it is possible to focus on the competitive behaviour between ions. SCM cannot predict CI: It is shown that SCM is accurate for low ionic strength, but for higher ionic strengths it becomes more unreliable [27, 31, 32].

2.3.2. Experimental Methods

One of the challenges of experimental methods that probe the properties of the EDL, is that it is difficult to do measurements on systems with a high concentration (>0.1 M). This has different reasons for different experimental methods. Because for divalent electrolytes the critical concentration is high, there is little experimental research that investigates divalent systems in the CI regime. The most used experimental techniques that are relevant for the research of confined electrolyte mixtures and their electrokinetic behaviour are discussed here.

Potentiometric titrations

Potentiometric titrations can be used to determine the bare surface charge density of the wall that is in contact with an aqueous electrolyte. For a known pH, the total concentration of available protons can be determined. The free amount of protons is known beforehand. The number of bound protons can be calculated by subtracting the free amount of protons from the total proton concentration. This can be used to determine the bare surface charge density [28]. Potentiometric titration methods are often combined with methods that can measure the concentration of a certain ion type, from which the adsorption uptake can be calculated. Several research groups have shown that the ionic strength, pH-value of the solution and bare surface charge are closely related. They combined potentiometric titrations with, for example, radiotracer technique [15, 17, 29, 33].

Radiotracer technique

By using radiotracer technique, it is possible to determine the adsorption uptake of a certain element in the solution if radioactive isotopes are used. By measuring the radioactivity of the isotopes before and after adding them to the system, the total uptake can be calculated[15, 29]. This can be used to compare the uptake of ions for different ion concentrations. Combined with potentiometric titrations the ion adsorption for different pH-values can be investigated.

Electrokinetic measurements

This group of experimental techniques imposes a condition, such as a pressure difference or an electric field which leads to transport of ions (current) and fluid. The electrokinetic phenomena on which they are based were previously described in section 2.2. Additional information is often obtained by using analytical coupling models such as the Helmholtz-Smoluchowski theory. Note that these theories rely on a set of assumptions, so caution should be taken when interpreting the results obtained with these models.

Streaming currents

In streaming current experiments, a pressure difference across a channel is applied, causing the electrolyte to move with a known flow profile. The imbalance of anions and cations in the EDL cause a net current, which is measured by electrodes. This is called the streaming current [1]. This experimental method cannot observe flow reversal.

Electrophoresis

In electrophoresis measurements, an electric field is applied to a system containing a free aqueous electrolyte with solid colloids. The movement of the colloids is determined by the EDL composition and can be measured, for example by measuring the frequency shift in light that is scattered by the moving colloids. The electrophoretic mobilities can then be used to derive the zeta potential [17, 27, 29].

Other experimental methods

Some other experimental methods give insight into the static properties of the electrical double layer and the surface and have been widely used. A few examples are atomic force microscopy (AFM) and methods that use X-rays to investigate the chemical composition of a sample. However, these methods are less suitable to probe high concentrations and/or electrolyte mixtures. They are still mentioned here to give insight into how research into the EDL is often conducted and why available data for electrokinetic mixtures in the CI regime is limited.

Atomic force microscopy

Atomic force microscopy uses a tip that is connected to a cantilever. The tip moves over the surface of interest, and the forces between the tip and the surface cause the cantilever to deflect. This method gives insight on the roughness and adsorption close to the surface with a nanometer resolution [24, 34, 35]. The residence time of ions in the Stern Layer has also been studied using AFM [36]. AFM is not suitable for high concentrations (0.1 M) as a dense electrical double layer leads to screening of the electrostatic forces close to the surface, so the force felt by the tip is altered [37]. AFM also cannot distinguish different molecules and ions, which makes it less suitable to investigate electrolyte mixtures. Surface force apparatus (SFA) is a similar experimental technique.

X-ray photoelectron spectroscopy and other X-ray based methods

X-ray photoelectron spectroscopy (XPS) is a technique often used to determine the quantitative chemical composition of a sample. An X-ray beam is emitted onto the sample, causing electrons to escape. The electronic excitation is measured, and from that, the chemical and electronic states of the material can be inferred. XPS can also be combined with other techniques for depth profiling. It has been used to investigate the depth and composition of the Stern layer [38, 39]. XPS and other methods that use X-ray beams are not suitable for high concentrations, as the X-ray beam might not be able to pass through the dense layers of atoms before reaching the Stern layer. Other methods using X-ray beams are for example in-situ anomalous X-ray reflectivity (RAXR) and X-ray diffraction. RAXR and X-ray diffraction can be used to measure the distance of adsorbed ions to the surface, allowing ions to be classified as ISSC or OSSC [16, 20].

2.3.3. Computational Methods

Experimental techniques can describe the macroscopic properties of a system, but it is very difficult to get microscopic information. Furthermore, it is challenging to probe both transport and structural properties at the same time using experimental methods. Molecular dynamic simulations on the other hand, can provide full access to the microscopic structure and dynamics. This information can ultimately be used to improve the analytical methods. In this thesis, MD simulations are used. Other computational methods, for example Monte Carlo simulations, rely on stochastic sampling of a system, which makes it less suitable to study the dynamic properties of a system. They are not discussed here.

Molecular dynamics simulations

Molecular dynamics (MD) simulations allow the events on an atomistic level to be studied without having to perform physical experiments. Newton's second law is time-integrated providing information on the positions, velocities and forces of each atom at every timestep. The parameters used to calculate the interatomic forces are defined in a force field. These force fields are empirically designed to be able to recreate certain macroscopic properties in a system.

One of the downsides of MD is the computing time. To illustrate: simulating 10 000 atoms for approximately 15 nanoseconds takes a day on 28 CPU's. This also compromises the system size that can be studied. System sizes of a few nanometers (1-20nm) are typical. This also limits the access to low concentrations of aqueous electrolytes as sufficient ion particles in the system are needed to obtain statistically meaningful data. The concentrations that are studied typically have an order of magnitude between 0.1 M and 1.0 M. This makes it hard to compare to experimental research, as experimental methods typically measure concentrations of two to three orders of magnitude smaller.

2.4. State of the Art

Research that investigates transport of electrolyte mixtures is limited. However, the electrical double layer properties for multivalent ions, ion competition in static systems and electrokinetic properties for multivalent solutions have been studied. These studies are also relevant for this research. This section describes their main findings. For a discussion of previous literature compared to this work, refer to section 5.3.

2.4.1. Prediction of the Structural Properties of the Electrical Double Layer

Van der Heyden *et al.* found that charge inversion decreases when monovalent KCl salt is added to a trivalent $CoSepCl_3$ electrolyte mixture by performing streaming current measurements. Kosmulski [15] has shown that calcium uptake decreases when sodium chloride is added to the system. This can also explain the decrease in charge inversion assuming that divalent calcium ions in the EDL get replaced by monovalent sodium ions [16]. However, the exact mechanism of charge inversion reduction remains a mystery. Ion competition and charge inversion are both not properly understood and no one-fits-all theory has been developed yet.

Several studies have attempted to modify the Poisson-Boltzmann Theory to improve the density profiles calculated [40, 41] such that they exhibit the same charge inversion as their simulations. However, they often use information from their molecular dynamics study directly as input for the adapted model. It is not possible to directly apply these adapted theories to other systems.

There are many mechanisms that contribute to adsorption of ions in the electrical double layer, many of which are not accounted for in the classical models. This is the reason that Poisson-Boltzmann Theory fails to predict charge inversion and ion competition. For example, the PB-theory only accounts for the electrostatic forces between ions and the surface. Szymanek *et al.* [17] showed that the adsorption behaviour of calcium and potassium on aluminium and silica surfaces are similar. Since aluminium has a positively charged surface and silica has a negatively charged surface, this means that only accounting for electrostatic forces between the ions and the surface is not sufficient.

Other mechanisms that contribute to adsorption, such as ion specifics and ion-ion correlations, have been researched. If they are properly understood, they can be used to refine models like the PB-model. The known shortcomings of the Poisson-Boltzmann model are discussed below to give an idea of what mechanisms and phenomena contribute to charge inversion and ion competition. Although not every assumption of the PB-model is relevant to this thesis, it does provide a clear framework in which this research is carried out.

Discrete surface charge

In the Poisson-Boltzmann model, it is assumed that the surface charge is uniformly distributed. This results in a decrease of the ISSC formation that is predicted, while ISSC's formation contributes strongly to CI [18, 42, 43]. Figure 2.9 visualises how a discrete surface charge can increase overscreening.

Figure 2.9: A visualisation of how discrete surface charge can lead to charge inversion. On the left: uniformly distributed surface charge, which is exactly screened by the counterions. On the right: discrete surface charges, which can cause overscreening.

.

Roughness of the surface

The roughness of the surface is not accounted for in the classical models. If the roughness of the surface is comparable to the width of the Stern Layer, the classical description of the EDL in planes is not valid anymore. Siboulet *et al.* [25] have shown this in a MD study electrolyte confined by amorphous silica. The roughness of the surface influences the accessibility of adsorption spots, which is visible in figure 2.10.

Ion specifics: size and hydration strength

If ion competition is present, then ion specific information becomes more important to account for. In the Poisson-Boltzmann model, the valency of the ions is the only ion specific characteristic that is taken into account. This would mean that higher valency ions are more likely to adsorb than lower valency ions. However, research has shown that other ion specific properties might be dominantly contributing to competitive adsorption.

For example, there might be spots on the surface that cannot be accessed due to the size of the ion [44]. Döpke *et al.* [18] showed that the hydration strength also plays a role in this steric hindrance: although divalent calcium ions experienced a higher electrostatic attraction from the surface, they also have a higher hydration strength due to their valency. Therefore, the water molecules can also form a steric hindrance, preventing the divalent ion to adsorb [20]. This is especially important for rough surfaces like amorphous silica. Hydration strength and ion size are different per ion species.

Figure 2.10: A visualisation of how surface roughness and ion specifics can contribute to ion competition. On the left, an example of adsorption on a flat surface. On the right, the bigger ion cannot access some of the spots on the amorphous surface. Note that the effect of hydration strength is not included.

Ion-ion correlations

The ions in the liquid also experience (electrostatic) interactions with each other. Strongly correlated liquid (SCL) theory is an adaptation of the Poisson-Boltzmann model which accounts for counterion-counterion correlations. Counterions are the ions that are oppositely charged to the surface charge. SCL states that for some systems it is energetically favourable to form a layer close to the wall with a higher counterion concentration than predicted by the PB-model [45, 46]. Van Der Heyden *et al.* [1] showed that SCL was applicable for his system with trivalent ions.

Co-ion - counterion interactions can also affect adsorption on the interface. Bjerrum pairing for example, occurs when a co-ion and a counterion form a complex together. This complex has its own valency and shape, which results in different adsorption behaviour than for the counterion alone. It is also possible that this increases the amount of anions in the EDL, which might increase flow reversal. Both Bourg and Sposito [19] and Lorenz and Travesset [47] have indicated in their MD studies that the pairing of mainly divalent (calcium) cations to chloride anions occurs in the EDL. Szymanek *et al.* [17] and Brugman *et al.* [20] combined their experimental findings with a surface complexation model. They both concluded that co-anion adsorption has to be accounted for in the SCM to make it fit onto their experimental data.

It depends on the surface type, ionic strength and ions present, to which extent co-ion - counterion and counterion - counterion are contributing to the structure of the EDL [43, 45].

Dielectric constant close to the wall

The dielectric constant is also called the relative permittivity. It is a measure of the polarizability of the solvent. Polarisation is related to the reorientation of molecules. This affects the interactions between particles. If a solvent has a high dielectric constant, the interaction between particles is less compared to a solvent with a low dielectric constant.

In the PB-model, the dielectric constant is assumed to be constant throughout the channel. However, it has been shown that the dielectric constant decreases close to the wall [48]. This affects the ion adsorption behaviour.

2.4.2. Prediction of the Electrokinetic Properties

There is little information about the electrokinetic behaviour of mixtures in the flow reversal regime. The study by Van Der Heyden *et al.* [1] suggests that charge inversion and presumably flow reversal can be suppressed by adding monovalent ions to a multivalent solution, although they did not directly measure the flow behaviour as the fluid motion is imposed by a pressure difference in the streaming current experiment. It is shown that charge inversion can be related to decreased mobility of the counterions in the EDL and thus an increased contribution of mobile co-ions, which contributes to flow reversal [22, 40]. Although it is clear that charge inversion and flow reversal are related, it is not exactly known how. There are examples of systems where charge inversion occurs, but flow reversal does not [49]. A clear explanation on which phenomena cause this is lacking and consequently there is no model that correctly describes the electrokinetic properties of a system that exhibits flow reversal.

Nonetheless, the findings by Van der Heyden *et al.* can be supported by an experimental electrophoresis study by Semenov *et al.* [12]. They researched the electrokinetic mobility of latex colloids in different solutions up to 1 M. The colloids have a negatively charged surface on which an electrical double layer forms. The size of the colloids is substantially larger than the EDL width, so the system can be considered as a flat, negatively charged surface that is in contact with an electrolyte. For increasing ionic strength, a mobility decrease of the colloid was observed and for the trivalent electrolyte, mobility reversal was found. However, for a mixture of trivalent lanthaan(III)chloride ($LaCl_3$) and monovalent potassium chloride (KCl), the mobility reversal decreased compared to a single $LiCl_3$ electrolyte. A study by Wang *et al.* [13] also found a mobility reversal reduction when ions of a lesser valency were added to a multivalent solution for DNA colloids. This shows that CI reduction and FR suppression are not unique to amorphous silica.

It is important to know that Semenov *et al.* [12] and Wang *et al.* [13] also found enhancement of mobility towards reversal when monovalent ions were added to a multivalent solution with a low concentration (below the critical concentration), although mobility reversal and supposedly charge inversion do not occur in these situations. Therefore, to find the CI reduction and FR suppression phenomenon, the initial multivalent concentration should be high. For lower concentrations, the electrostatic interactions between ions and the surface increase the screening of the surface, and ion-ion correlations play a smaller role because the ions are further apart on the surface.

SCL theory has been used to predict CI in trivalent solutions [1, 12, 14], taking into account ion-ion correlations. However, for divalent solutions this was not possible. This indicates that the mechanisms driving ion adsorption in trivalent mixtures in the CI regime are different from the mechanisms causing CI in divalent mixtures. This could also lead to different ion competition in mono-trivalent and mono-divalent mixtures. When our work is compared to the work studying mono-trivalent mixtures, this should be kept in mind.

There are no experimental studies that found CI reduction and FR suppression for mixtures of divalent-monovalent electrolytes, due to the inability of many experimental research methods to probe high ionic strengths. However, divalent-monovalent mixtures have been investigated. Thanh *et al.* [50] determined the zeta potential for mixtures of monovalent sodium chloride (NaCl) and divalent calcium sulfate ($CaSO_4$) in a system with a silica-based rock surface. They kept the ionic strength the same while increasing the fraction of calcium sulfate, so the total concentration goes up. The absolute zeta potential decreased when the proportion of divalent ions increased in the mixture. This means that the flow reversal tendency enhances, which opposes the findings by Van der Heyden *et al.*. Szymanek *et al.* [17] did a similar experiment in which they found FR enhancement when calcium chloride was added to potassium chloride. Szymanek *et al.* and Thanh *et al.* both varied the multivalent concentration, instead of the monovalent concentration. On top of that, they did not probe in the regime of charge inversion and flow reversal. This makes it difficult to test their work against our hypothesis.

The trend of increasing flow reversal for increasing ionic strength reappears in an MD study by Prakash *et al.* [51]. This study considers the electroosmotic flow properties for mixtures of $MgCl_2$ and NaCl and $CaCl_2$ and NaCl for higher concentrations (0.1M). It was shown that the addition of divalent electrolyte to monovalent electrolyte leads to an increase in flow reversal and charge inversion. Unfortunately, the monovalent electrolyte in this study was also not varied against a set divalent concentration. Again, the importance of carefully selecting the concentrations that will be simulated in this work is accentuated.

There are a few factors that hamper the prediction of the velocity profiles along the channel using continuum theory. First of all, the Navier-Stokes equation (equation 2.9) requires the density profile as an input. As discussed in section 2.4.1, predicting an accurate density profile is complicated due to multiple mechanisms and properties that aren't fully understood yet. Other factors that complicate predicting the electrokinetic properties include assumption of a constant viscosity along the channel and a difficulty in predicting the location of the shear plane, which is needed as input to solve equation 2.9. These three factors are discussed below.

Structural properties as input

Van Der Heyden *et al.* [1] used SCL theory to predict charge inversion. This was successful for trivalent solutions, but not for trivalent-monovalent mixtures. Semenov *et al.* [12] confirmed that ion-ion correlations have a more dominant contribution to mobility reversal than discretized surface charge. They also concluded that ion specific effects should be accounted for to capture mobility reversal suppression when monovalent ions are added to the solution. Furthermore, Celebi *et al.* [49] and López-García *et al.* [52] have shown that including size-effects can lead to an improvement in the prediction of electrokinetic properties.

Viscosity enhancement

Continuum theory assumes the viscosity along the channel to be constant. However, if ions adsorb at the interface, this enhances the viscosity in the Stern layer. Hartkamp *et al.* [40] showed that the prediction of the electrokinetic properties improve if this viscosity enhancement is included in equation 2.9.

No shear plane

The zeta-potential is the electric potential at the shear plane. In continuum theory, the shear plane is defined as the position where the velocity profile is zero. According to the classical models, the shear plane is located between the Stern layer and the diffuse layer. It also has been suggested that for amorphous silica, a stagnant diffuse layer exists which would move the location of the shear plane and thus alter the zeta potential [53]. Experimentally finding the location of the shear plane remains difficult [38, 54, 55]. MD research even shows that a clear distinction between a stagnant and mobile layer is nonexistent, so no shear plane can be defined at all [25]. This implicates that the interpretation of experimental data of the zeta potential should be carefully considered. It also complicates comparison between data from molecular dynamics and experimental data[56].

3

Methodology

This section describes the methodology used to obtain the results in this thesis. Common elements of Molecular Dynamics (MD) are discussed in Section 3.1. The specific simulation setup is explained in Section 3.2. Section 3.3 describes the post-processing methods that are used.

3.1. Molecular Dynamics

This section explains the basic principles of MD Simulations, starting with how Newton's second law of motion is solved. Afterwards, the interactions between particles are described and periodic boundary conditions and minimum image convention are explained.

3.1.1. Solving Newton's Second Law of Motion

In molecular dynamics simulations, Newton's second law of motion as shown in equation 3.1 is numerically solved. In this thesis, we use the Velocity Verlet algorithm to solve the equations of motion to obtain the new position, velocity and force vectors for each particle. The new position $\mathbf{r}$ for each particle i after one time step can be calculated using the current position, velocity and force according to equation 3.2. The new force is derived from the total potential energy between particles as described by equation 3.3. The potential energy U exists of the interaction energy between particle i and the other particles in the system as described in Section 3.1.2. The new velocity $\mathbf{u}$ is calculated by using the current and the new force following equation 3.4.

$$\mathbf{F} = m\frac{d\mathbf{u}}{dt} \tag{3.1}$$

$$\mathbf{r}_i(t+\Delta t) = \mathbf{r}_i(t) + \mathbf{u}_i(t)\Delta t + \frac{1}{2m_i}\mathbf{F}_i(t)(\Delta t)^2 \tag{3.2}$$

$$\mathbf{F}(t+\Delta t) = -\nabla U \cdot \mathbf{r}(t+\Delta t) \tag{3.3}$$

$$\mathbf{u}_i(t+\Delta t) = \mathbf{u}_i(t) + \frac{\mathbf{F}_i(t) + \mathbf{F}_i(t+\Delta t)}{2m_i}\Delta t \tag{3.4}$$

3.1.2. Interactions between Particles

The interaction energy between particles consists of bonded and non-bonded interactions as described by equation 3.5. The non-bonded interactions can be decomposed into the Lennard-Jones (LJ) interactions and the electrostatic interactions, depicted by the first two lines in equation 3.5. The bonded interactions are the harmonic interactions for bonds and angles as shown in the last line of equation 3.5. Note that the non-bonded interactions are not calculated for 1,2 and 1,3 ion pairs. This means that directly bonded pairs in for example silica (Si-O) or indirectly bonded pairs with one atom in between (Si-O-Si) are not considered. The individual terms of equation 3.5 are discussed in this section.

$$
\begin{aligned}
U = & \sum_{ij,nonbonded 1,2 and 1,3 excl} 4\epsilon_{ij}\left[\left(\frac{\sigma_{ij}}{r_{ij}}\right)^{12} - \left(\frac{\sigma_{ij}}{r_{ij}}\right)^{6}\right]_{(Lennard-Jones)} + \\
& \frac{1}{4\pi\epsilon_0} \sum_{ij,bonded 1,2 and 1,3 excl} \frac{q_i q_j}{r_{ij}}_{\ (Electrostatic)} + \\
& \sum_{ij,nonbonded} K_1(\mathrm{r}-\mathrm{r}_0)^2_{(Bonds)} + \sum_{ijk,bonded} K_2(\theta-\theta_0)_{(Angles)}
\end{aligned} \tag{3.5}
$$

Lennard-Jones Potential

The LJ potential (first line in equation 3.5) describes the Van der Waals attraction (^{6} term) and Pauli repulsion (^{12} term) as a function of distance **r** between two particles as shown in figure 1.1. The repulsive part originates from overlapping electron clouds as two particles move closer to each other. σ_{ij} is the Lennard-Jones diameter, which is the finite distance where the potential between atoms is zero, so at r_{ij}/σ_{ij} is 1 in figure 3.1. ϵ_{ij} is the energy parameter, which is the depth of the potential energy well. Because the LJ potential approaches zero fast, a cut-off distance is often introduced to decrease computation time.

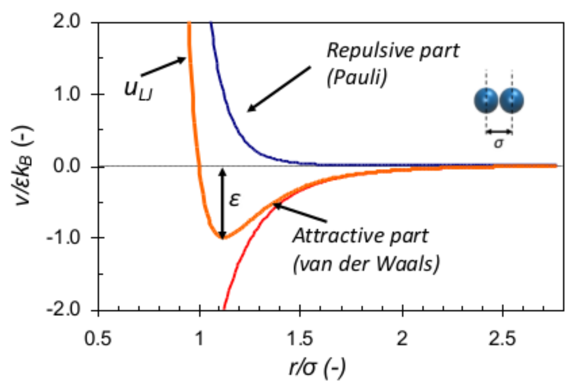

Figure 3.1: The Lennard-Jones potential, including the parameters σ_{ij} and ϵ_{ij}.

Electrostatic Potential

Equally charged particles experience a repulsive electrostatic force, whereas oppositely charged particles experience an attractive electrostatic force towards each other. This is described by the electrostatic potential between the two particles i and j as seen in the second term of equation 3.5. The particles are considered to be point charges with charge q at a distance r. ϵ_0 is the dielectric permittivity of a vacuum.

Bonds and Angles

Bonds stretching and angle bending can be described by a harmonic potential as depicted by the last two terms in equation 3.5 respectively. K is the spring stiffness and θ the angles between the bonded particles.

3.1.3. Periodic Boundary Conditions and Minimum Image Convention

Due to the limited size of MD simulations, periodic boundary conditions (PBC) are usually applied. The simulation box with particles and their velocities is copied in all directions as shown by the 2D schematic in figure 3.2. If a particle leaves the box on top, a copy will enter the box on the bottom. Along with PBC's, minimum image convention is often used. This means that particles only interact with the nearest copy of another particle, as shown in figure 3.2.

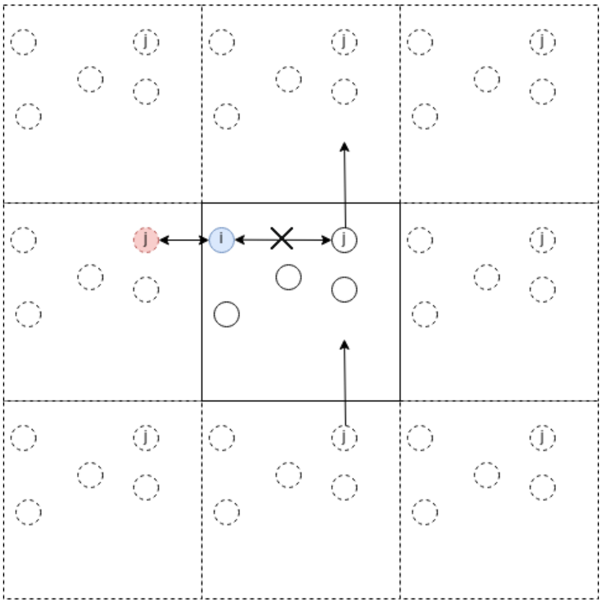

Figure 3.2: The periodic boundary condition visualized, including minimal image convention.

3.2. Simulation Setup

Large-scale Atomic/Molecular Massively Parallel Simulator (LAMMPS) software is used to run the molecular dynamics simulations. This section contains all information needed to run the simulations carried out in this thesis. First, the topology of the system is described. Secondly, the force fields used are explained. Finally, the initialization and production process and all relevant parameters are given.

3.2.1. Topology

The simulation box has a size of 35 by 35 by 107 Ångstrom. It consists of two silica walls, with a channel in the middle that consists of water molecules and ions. The initial configuration for one of the simulations carried out in this experiment is shown in figure 3.3.

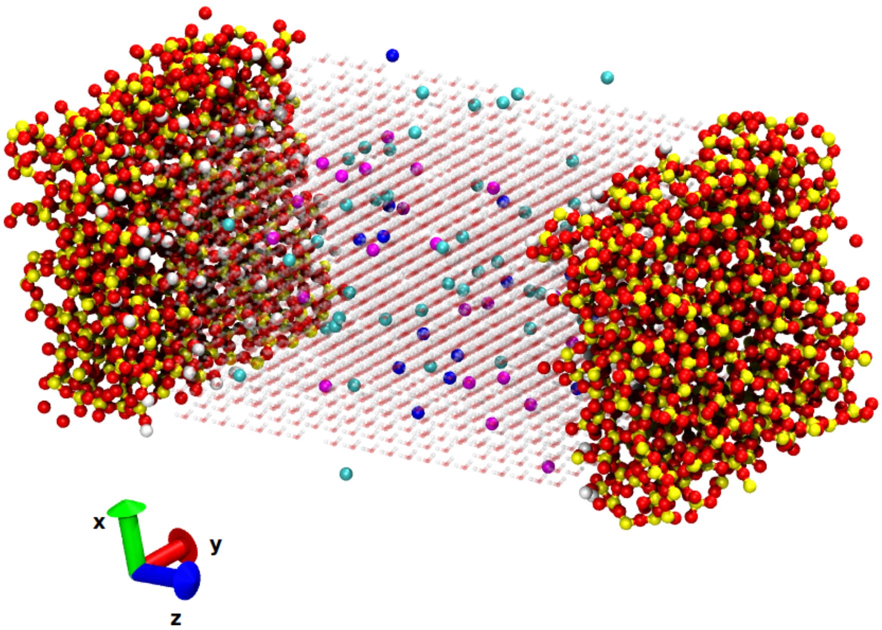

Figure 3.3: The simulation box with the silica confinement and water molecules and calcium, chloride and sodium ions.

The water molecules are added to the system in an orderly manner with a target density of 1 g/L. Nonetheless, due to the amorphous structure of the surface and resulting ambiguity of available volume for the fluid, the density was further adjusted during initialization as described in section 3.2.3.

Van Der Heyden et al. have found that 0.4 mole/L (M) is the critical concentration for calcium chloride [1]. Therefore, 4 systems were created with a fixed $CaCl_2$ bulk concentration of 0.4 M and a varying NaCl bulk concentration from 0 to 0.7 M as shown in table 3.1 and visualized in figure 3.4. The bulk is defined as the region in which the velocity is constant, which in our case is a region of 3 nm in the middle of the channel. Note that due to finite size affects the number of calcium ions was lowered at increasing NaCl concentration to keep the bulk concentration of $CaCl_2$ constant. This was found to be necessary since fewer calcium ions adsorb at increasing NaCl concentration which would otherwise lead to an increase in $CaCl_2$ concentration.

Table 3.1: The number of ions in the system per concentration.

Name	Ca	Na	Cl	Ca [M]	Na [M]	Cl [M]
0.0M NaCl	24	0	32	0.405	0.00	0.836
0.2M NaCl	22	14	42	0.421	0.249	1.11
0.5M NaCl	20	26	50	0.403	0.480	1.30
0.7M NaCl	18	38	58	0.396	0.716	1.51

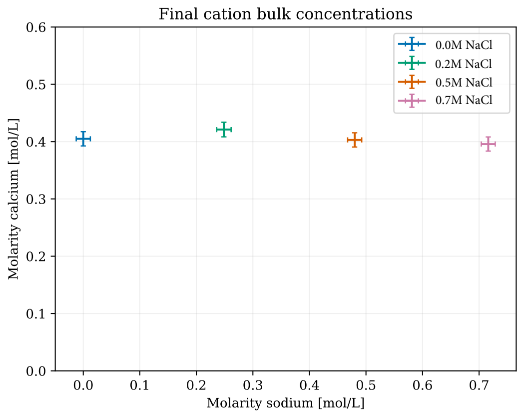

Figure 3.4: The final concentration of each simulation after initialization.

The same silica channel is used as the one created by Döpke et al. in both of his studies from 2019 and 2021 [18, 57]. In short, an amorphous silica block is created and split in two while making sure that the bulk silica density and the surface silanol density are similar to experimentally confirmed values. The silica blocks are then moved apart to a distance of 6 nm, forming a confinement.

Figure 3.5 shows the number of deprotonated sites needed per wall to obtain a realistic bare surface charge density for this system size at a pH-value of 7.5. For a calcium chloride concentration of 0.4 M, 8 deprotonation sites are needed. Figure 3.5 contains the experimentally found bare surface charges for single electrolytes only. It is unknown what the bare surface charge exactly should be for mixtures. Roughly interpolating between 0.4 M $CaCl_2$ and 0 to 0.7 M NaCl results in a deprotonation number of 7 or 8. To investigate the effect of the concentration and surface on the simulations, the deprotonation number preferably is the same for each concentration. This leads to a choice of eight deprotonation sites per wall, resulting in a bare surface charge density of -104.5 mC/m^2.

To generate the deprotonation configuration, a million random combinations of possible deprotonated silica groups are generated. The configuration that has the largest average distance between the deprotonated sites is chosen.

3.2.2. Force Fields

The parameters (ϵ_{ij}, σ_{ij}, mass and charge) used to calculate the interatomic potentials are stored in a forcefield. This thesis uses the Interface Force Field (IFF) for silica [58] and Madrid-2019 for the ions [59], which also includes the TIP4P/2005 water model. The parameters can be found in appendix A.

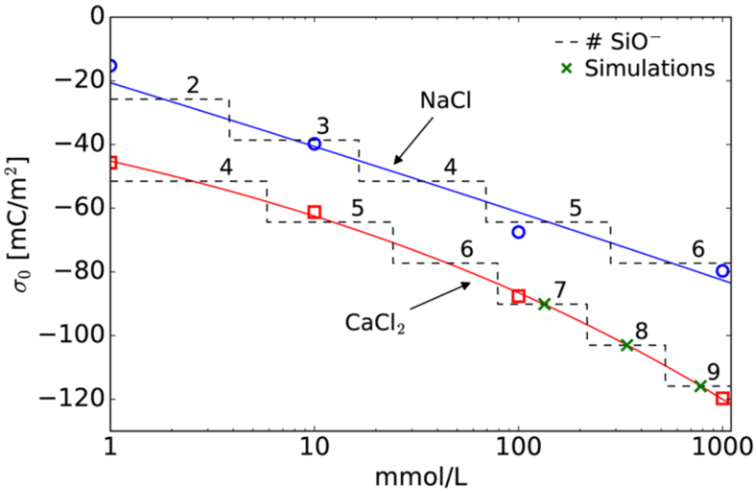

Figure 3.5: The amount of deprotonated sites per wall needed to obtain the correct bare surface charge density at a pH of 7.5. The amount of deprotonated sites is valid for a silica wall of 35 by 35 ångstroms. Figure taken from [57].

While these force fields are originally not developed and optimized for each other, Döpke and Hartkamp [57] have shown that scaling the interaction between the oxygen atoms of silica and the ions improves the adsorption properties for a system of calcium chloride. Therefore, the same scaling between silica oxygens and ions is used. The scaling is shown in equation 3.6, where the scaling factor f for calcium is 0.9. For chloride and sodium, a scaling factor of 1.0 is used. A can denote σ or ϵ, X is either Ca^{2+} or Na^{+}.

$$A_{X_{OIFF}} = A^{LB}_{X-O_{IFF}} \left[\left(\frac{A_{X-O_{water}}}{A^{LB}_{X-O_{water}}} - 1 \right) f + 1 \right] \tag{3.6}$$

The cutoff distance used to calculate both Lennard-Jones and Coulombic interactions is 12 Å. For the long-range electrostatic interactions, a particle-particle particle-mesh solver was used with an accuracy of 10^{-4}.

3.2.3. Simulation Parameters

For each concentration in table 3.1, three independent simulations were performed with different starting conditions and deprotonation configurations. Each simulation consists of an initialization run of 45 nanoseconds and a production run of 25 nanoseconds. Throughout the complete simulation, the angles and bonds within silica and water molecules were fixed using the SHAKE algorithm with an accuracy of 10^{-4}. A periodic boundary condition was applied in all directions. The PBC in z-direction is combined with a vacuum boundary condition as described by Yeh and Berkovitz [60]. Next to the silica walls, a vacuum that is three times the simulation box size is introduced. This prevents long-range electrostatic interactions between the simulation box duplicates in z-direction.

Initialization

During the initialization, the complete system was in a canonical ensemble (NVT) with a temperature kept at 298 K via a Nose-Hoover thermostat. The first step during initialization is to acquire the correct fluid density in the system. This was done by applying a force to the outer walls that equals 1 atm. The walls move towards each other until a realistic density for a pressure of 1 atm is reached, after which they were fixed in space. This was done with a timestep that increased until it was 2 femtoseconds.

When the electric field was applied, the fluid in the system was in the microcanonical ensemble (NVE). To keep a constant temperature in the system, the walls were kept connected to a heat bath of 298 K via a Nose-Hoover thermostat. During equilibration, the electric field was gradually applied to the system. The final strength of the electric field was 0.5 V/nm. An equilibration time of 45 ns was chosen, which is comparable to the equilibration time by Prakash *et al.* [51] who had a similar electric field magnitude.

The electric field strength in experimental work and in nanofluidic devices is in the order of magnitude of V/cm, whereas the electric field strength in our work is 0.5 V/nm. Such a large electric field strength is needed to obtain a good signal-to-noise ratio for the electrokinetic properties. For our results to be valid in the experimental regime, it should be checked that the EOF and the electric field strength scale linearly. This was done by running one simulation at 0.25 V/nm. Figure 3.6 shows the linearity of the relative velocity of the ions and figure 3.7 shows that the adsorption behaviour is independent of the electric field strength. From this, we conclude that the system is running in the linear regime.

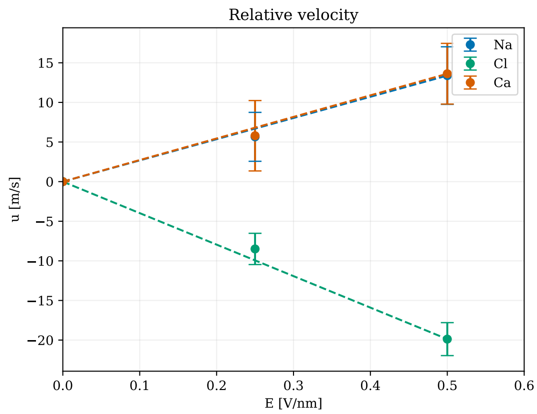

Figure 3.6: The relative ion velocity in the bulk for an electric field of 0.25 V/nm and for 0.5 V/nm. The error bars are within 68% certainty.

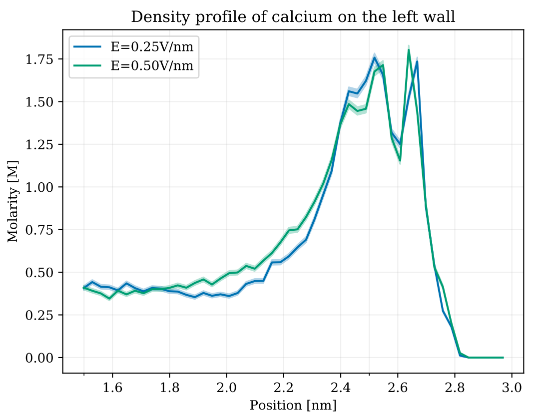

Figure 3.7: Calcium adsorption for an electric field of 0.25 V/nm and for 0.5 V/nm.

Production

The production run lasts 25 ns with a time step of 2 fs. From figure 5.6 it was concluded that this is enough data to represent our sample. Every 2000 fs, or each 2 ps, data from the simulation is stored.

3.3. Post-Processing

For each concentration three independent simulations were performed with a different surface configuration on both walls and with a different starting configuration of the ions. This means there are six datasets (three simulations with two walls) that are averaged to obtain the results. This section describes the post-processing of the data performed to obtain the results in the next chapter.

Uncertainty

The uncertainty between individual frames for single datapoints is neglected, as this data is highly correlated. The standard error within 68% certainty between the left wall and right wall of all three simulations is calculated according to equation 3.7. There are six datasets j for each datapoint i. This method is followed for all data unless stated otherwise.

$$error_i = \frac{\sqrt{\sum_{j=1}^{6}(x_j - x_{mean_j})^2}}{\sqrt{6}} \tag{3.7}$$

Position of the wall

The position z of the wall is assumed to coincide with the position at which the water density has decreased to one sixth's times the bulk value. Note that in reality, the wall is a rough surface.

Distance to the nearest wall atom

To distinguish between the different ion types (ISSC, OSSC, DS and FI), the distance d to the nearest wall atom can be used, instead of the position z normal to the wall.

Screening function

Equation 2.1 is used to obtain the screening profiles as a function of z.

Adsorption over time

The adsorption number of each ion type is determined by calculating the distance between each ion to the closest wall atom. The distance determines the ion type as described in table 3.2. The ISSC and OSSC are plotted over time. The average is taken for every 0.2 nanoseconds.

Table 3.2: Ion type determination.

Ion type	**Distance [Å]**
ISSC	<3.0
OSSC	<5.25
DS	<12
FI	> 12

Electroosmotic flow over time

The electroosmotic flow over time is plotted. The electroosmotic flow is calculated by taking the average velocity in the middle of the channel: between -1.5 nm and 1.5 nm in figure 5.13. The average is taken for each 0.2 nanoseconds. To calculate the error of the mean for the electroosmotic velocity, equation 3.8 is used. The error bars are omitted for clarity.

$$err_{combined} = \frac{\sum_i^N (\sigma_i^2 + (\mu_i - \mu)^2)}{N} \tag{3.8}$$

Zeta potential

The zeta potential is calculated using equation 2.13. The values in table 3.3 are used. Note that the temperature is taken as the average along the channel. The viscosity follows from the temperature and figure 3.8

Table 3.3: Parameters to calculate ζ and the shear plane location.

Ion type	**Value**
T	309.7 K
η	$6.65 \cdot 10^{-4}$ Pa.s
ϵ_0	$8.85 \cdot 10^{-12}$ C^2/Jm
ϵ_r	60
E	0.5 V/nm
σ	-104.5 mC/m^2
e	$1.6021 \cdot 10^{-19}$ C

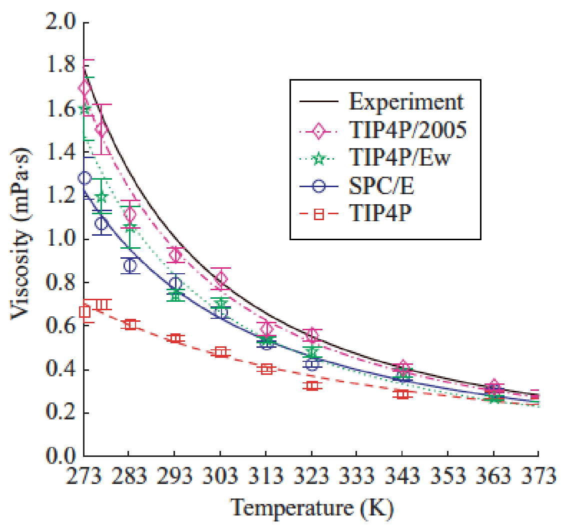

Figure 3.8: The relation between viscosity and temperature. Taken from Markesteijn et al [21].

Shear plane location

To find the location of the theoretical shear plane, first the electric potential is calculated by solving equation 2.8 with boundary conditions 2.6 and 2.7. This is done by discretizing Poisson's equation using the finite differences method. The density profile from the

MD simulations is used as input. The location of the theoretical shear plane is located at the intersection between the electric potential and the zeta potential from the Helmholtz-Smoluchowski equation. The parameters used to solve Poisson's equation can be found in table 3.3.

Ion transport diffusion

The ion transport diffusion is calculated using the same method as Döpke and Hartkamp [18]. For each ion species s and adsorption type a the diffusion can be calculated using equation 3.9. The ion transport diffusion coefficients are calculated with equation 3.10 where the electric ion mobility is found with equation 3.11. z is the ion valency, ρ_n the number density, and v and E are the velocity and electric field strength in x-direction.

$$D_{ia} = \frac{\int \rho_n(z)_{ia} D(z)_{ia} dz}{\int \rho_n(z)_{ia} dz} \tag{3.9}$$

$$D_{ia}(z) = \frac{\mu_{ia}(z) k_b T}{ze} \tag{3.10}$$

$$\mu_{sa}(z) = \frac{u_{ia} - u_{water}(z)}{E} \tag{3.11}$$

4
Verification

This paragraph contains the verification of the simulations done with solely calcium chloride. By this mean it is checked whether the simulations and data analysis are performed correctly. The data is compared to the molecular dynamics work by Döpke and Hartkamp [57], as the concentration and simulation conditions are the same. The data from our work contains 3 independent simulations of 25 nanoseconds. The data from Döpke and Hartkamp contains 2 independent simulations of 100 nanoseconds. For all data, the average between the left and the right wall is taken as they have a different configuration.

4.1. Structural Properties

The final mass density of the electrolyte in the bulk can be found in table 4.1. It is within the same range as what other sources have reported.

Table 4.1: The mass density of our simulation compared to other sources.

Mass density [kg/m^3]	**Source**
1027.3 ± 3.77	0.0M NaCl
1024	[57]
1031	[61, 62]

The final concentration of calcium along the channel can be found in figure 4.1b. The molarity in the bulk is the same for both our simulation and the data from Döpke and Hartkamp, which makes this data suitable for comparison with our simulations. The adsorption in the EDL and consequently the screening function are very similar as seen in 4.1.

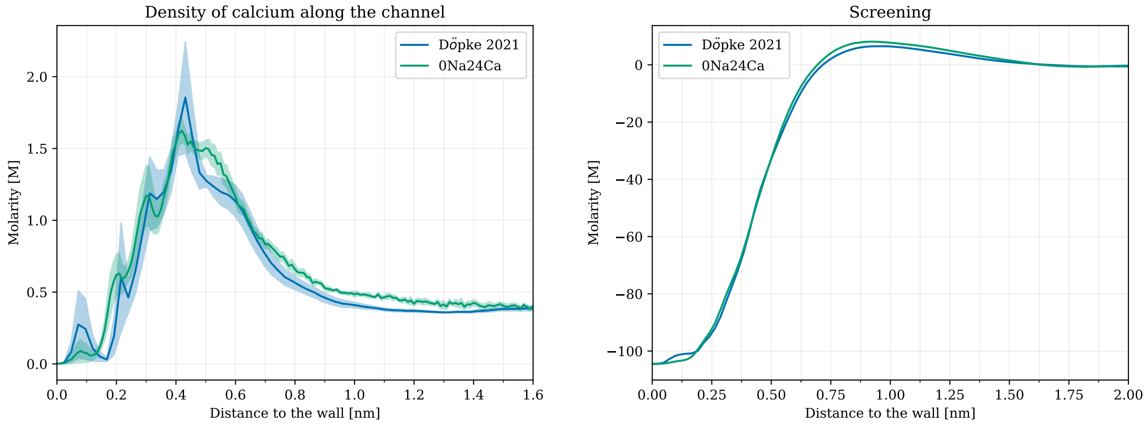

(a) The calcium adsorption in the EDL.

(b) Calcium density along the channel.

Figure 4.1: Verification of the structural properties.

4.2. Electrokinetic Properties

Figure 4.2 shows the temperature of the channel after application of the electric field and the equilibration time of 45 ns. A temperature increase in the channel is seen whilst the walls are kept at a constant temperature of 298 K. The temperature increase will cause a viscosity decrease [21]. The viscosity in the EDL impacts the EOF velocity in the bulk due to the shear stresses between mobile and less mobile particles. A temperature increase will therefore lead to a velocity increase of water. The comparison of the results for each simulation is not affected as the temperature increase is small and the same for each simulated system.

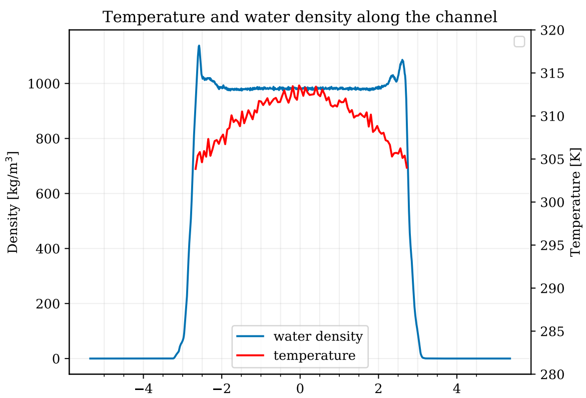

Figure 4.2: The temperature and the water density along the channel.

In our simulation, an electric field of 0.5 V/nm was used, whereas Döpke and Hartkamp used an electric field of 0.2 V/nm. The system from the work of Döpke and Hartkamp does not have a temperature in the bulk. Figure 4.3 shows the velocity profiles for which the velocity of our simulations is scaled to match the electric field of the other data. The chloride velocity is in good correspondence. The calcium velocity of our simulations is slightly higher. This may be caused by weaker adsorption of cations in the EDL, which can be

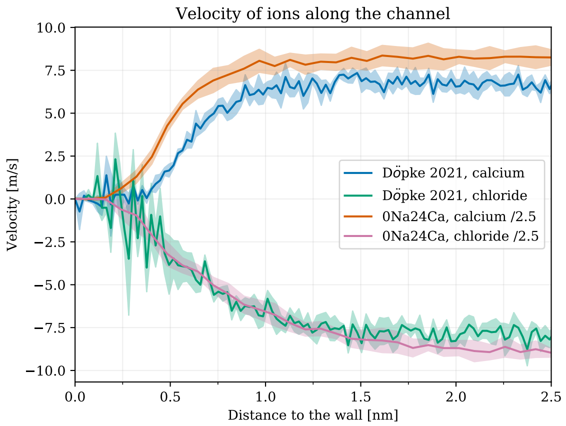

(a) Ion velocity.

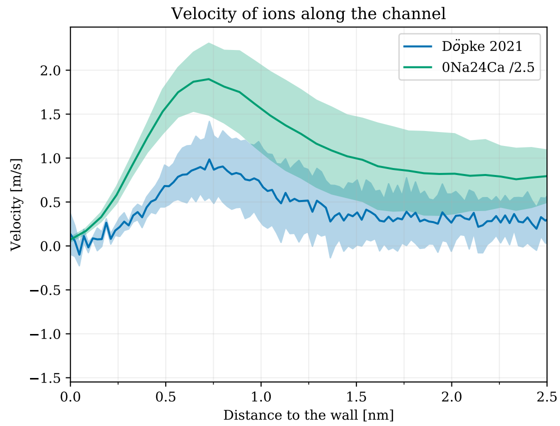

(b) Water velocity.

Figure 4.3: Verification of electrokinetic properties.

caused by the temperature increase. The water velocity is also higher, which can be caused by the viscosity decrease. In section 3.2 it was explained that the linear scaling is still within acceptable ranges. Figure 4.4 shows the zeta potential, which is in good agreement with Van Der Heyden *et al.* [1] and Döpke and Hartkamp [57].

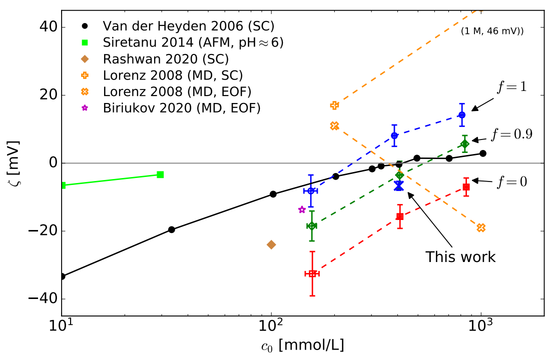

Figure 4.4: The zeta potential from different sources. Figure adapted from [57].

5

Results and Discussion

This thesis aims to find out if the transport of a calcium chloride ($CaCl_2$) solution can be controlled by adding sodium chloride (NaCl). Literature shows that adding monovalent ions to a multivalent solution leads to charge inversion reduction and flow reversal suppression, suggesting that the transport can be controlled. We found that for our concentrations, this is not the case. This chapter presents these results and investigates why the phenomena found in other research do not occur in our work. In section 5.1 the effect of adding NaCl to $CaCl_2$ on the structure of the EDL is discussed. The impact on the electrokinetic properties and its relation to the structural properties of the EDL are investigated in section 5.2 t. Section 5.3 places our findings in the context of previous research on electrokinetic properties of electrolyte mixtures. Finally, a discussion is held about the most important assumptions and their implications in this thesis in section 5.4.

5.1. Structural Properties

In this section, the structural properties of the EDL for our electrolyte mixtures are presented. It is shown that charge inversion is not suppressed for the simulated concentrations. The adsorption of different ion species is discussed to explain why the screening profile does not show this trend.

5.1.1. Screening

The screening profile for all concentrations is shown in figure 5.1. There is no clear distinction between the charge inversion magnitude for each concentration; the difference is within uncertainty. This is not in line with the CI reduction that Van Der Heyden *et al.* [1] found when KCl was added to a trivalent CoSep solution. There is also no increase in CI, which could be expected from increasing ionic strength. Increasing CI for increasing ionic strength is what was found for the work by Bourg and Sposito [19] who studied similar concentrations for NaCl and $CaCl_2$ on smectite surfaces.

Another observation is that the increasing slope shifts closer to the wall when more sodium is added to the electrolyte because sodium adsorbs closer to the wall than calcium. Furthermore, the slope between the peak of the screening function and z=1.6 nm becomes steeper for increasing sodium concentration because there is relatively more chloride present in that region, which will be shown in section 5.1.2

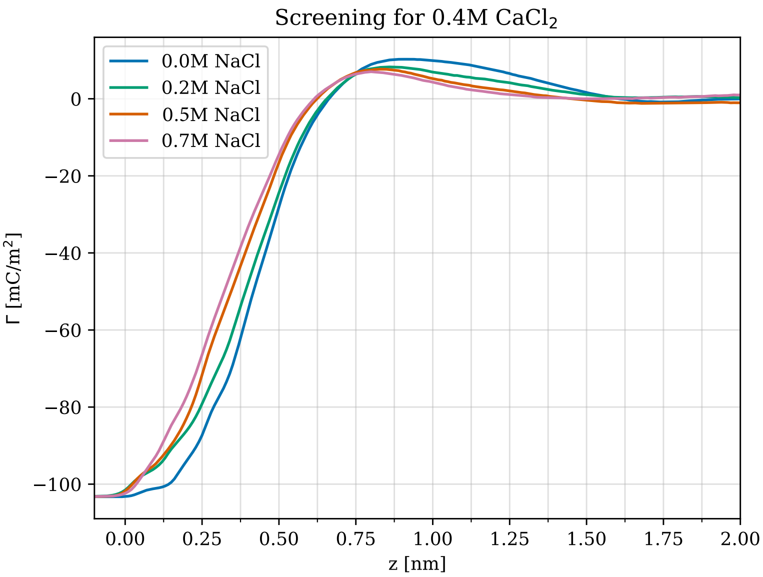

Figure 5.1: The screening profile for all concentrations.

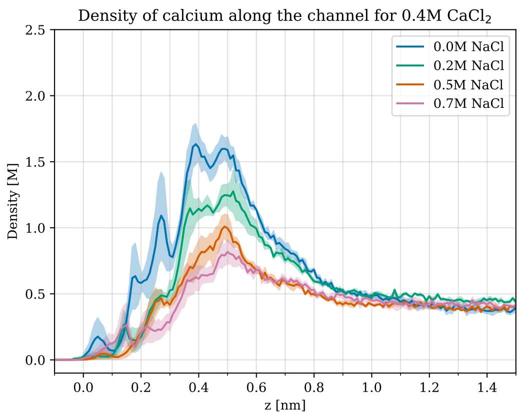

(a) Density of calcium.

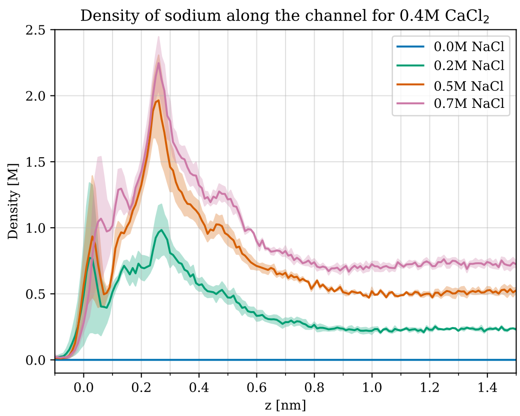

(b) Density of sodium.

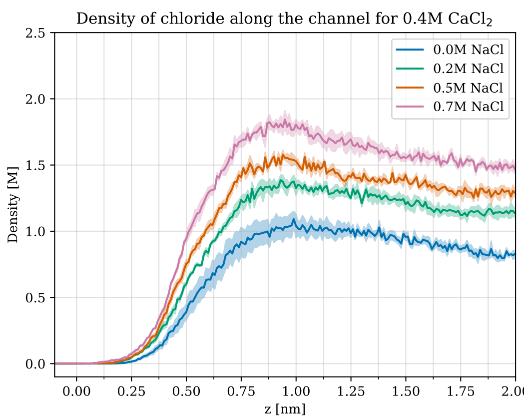

(c) Density of chloride.

Figure 5.2: The density profile for each ion species.

5.1.2. Density profile

Figure 5.2 shows the density profiles for calcium (Ca^{2+}), sodium (Na^{+}) and chloride (Cl^{-}) ions. It can be observed that Ca^{2+} adsorption reduces for increasing NaCl concentration. Especially close to the walls the calcium ions are replaced by sodium ions, which is depicted by the difference in width between the blue line and the other lines in figure 5.2a. Furthermore, sodium ions seem to adsorb closer to the surface as seen in 5.2b. This is also the cause of the shift of the peak in the screening function towards the surface in figure 5.1. Finally, due to the increase in NaCl concentration, the amount of overall chloride ions increases as shown in figure 5.2c. Note that the diffuse region of Cl^{-} also becomes more pronounced with increasing NaCl concentration. This explains why the screening function goes to zero faster for the higher NaCl concentrations.

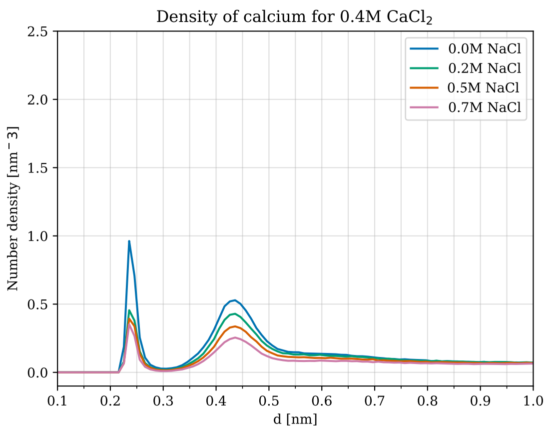

(a) Calcium density.

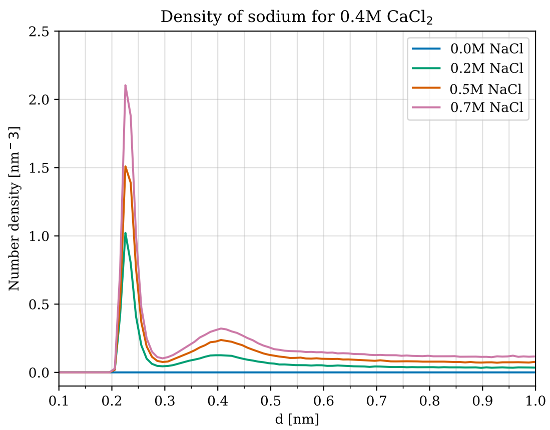

(b) Sodium density.

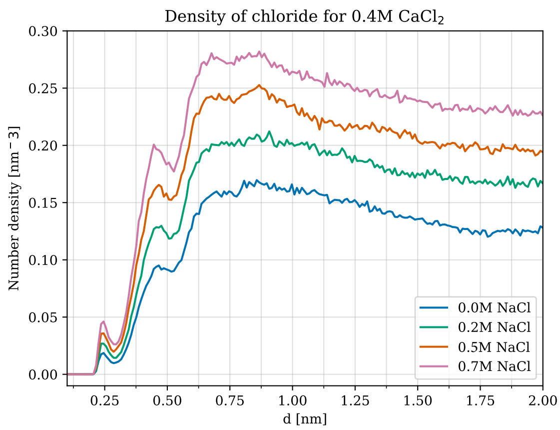

(c) Chloride density.

Figure 5.3: The density profile for each ion species against d.

To get a better insight into the adsorption of ions as ISSC, OSSC or diffuse species, the distance to the nearest wall atom for all ions is analysed as shown in figure 5.3. First, the ISSC and the OSSC adsorption of cations will be discussed separately. The observations found for individual ions will be related to the total ion density and the charge density which are found in figure 5.4. Then the observations of the ISSC and OSSC adsorption are related to the screening function. Finally, the anions will be discussed.

Figure 5.3a shows that the ISSC formation of Ca^{2+} reduces by 53% when 0.2 M NaCl is initially added to the system. The decrease of Ca ISSC between 0.2 M and 0.5 M Na is 15% and the decrease between 0.5 M and 0.7 M Na^+ is 12%. At the same time, the formation of sodium ISSC increases with a magnitude between 40 to 50% for each concentration increase of sodium as shown in figure 5.3b. For a bulk concentration of 0.4 M $CaCl_2$ and 0.2 M NaCl, twice as much ISSC Na^+ is already formed compared to ISSC Ca^{2+}. It is clear that sodium ions outcompete calcium ions in ISSC formation.

One of the mixtures that Bourg and Sposito [19] studied was similar to our 0.7 M NaCl and 0.4 M $CaCl_2$ concentration. They studied 0.8 M NaCl and 0.3 M $CaCl_2$ for a smectite surface in an MD study with a system of similar size. They did not find the tendency of sodium ions to outcompete calcium ions. This emphasizes the effect that surface type has on adsorption. Smectite has a smooth and regular surface, whereas amorphous silica has a considerable surface roughness. This can cause adsorption spots and surface groups to be sunken into the surface, which leads to sterical hindrance for calcium ions due to their strong hydration shell [18]. Sodium ions have preferential adsorption on these spots, which can explain why sodium ions outcompete calcium ions for ISSC formation. Other spots that are protruded from the surface are easily accessible to calcium. This would explain why the decrease of calcium ISSC between the different mixtures is smaller than the initial decrease of 53% when sodium was first added [57].

Another difference between smectite and amorphous silica is that smectite does not have charged surface groups that are directly in contact with the liquid. Instead, smectite forms charge layers inside the wall material [63]. This results in little ISSC formation on the smectite surface, so the electrostatic force between the surface charge and the ions is too small to disrupt the hydration shell for strongly hydrated ions like calcium. Sodium ions also form little ISSC on smectite [19, 64]. Therefore, calcium and sodium ions adsorb further away from the surface than in our system, which is another reason why surface effects are not dominant in the study by Bourg and Sposito.

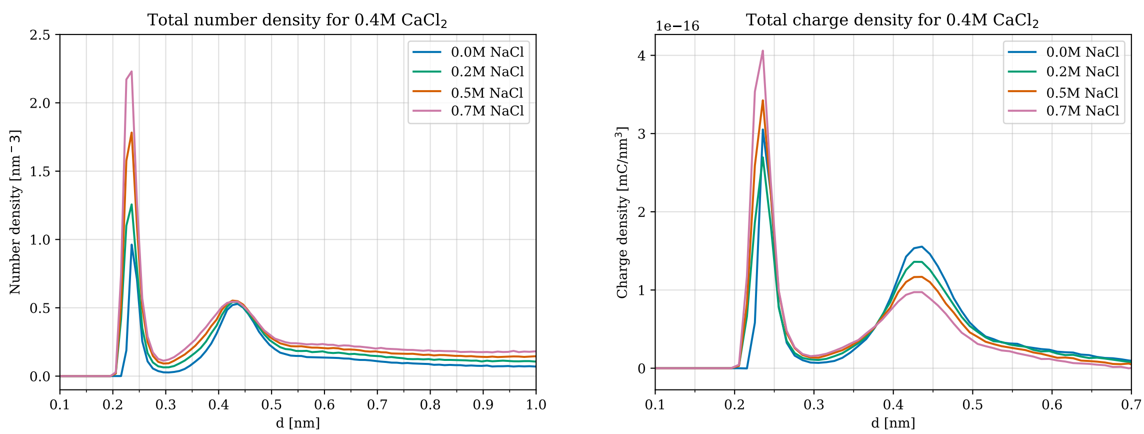

(a) The total ion density.

(b) The total charge density.

Figure 5.4: Total density properties against d.

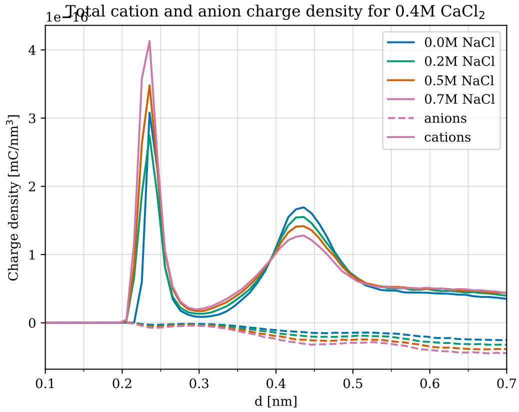

Figure 5.5: The total charge density for anions and cations.

Looking at figure 5.4a, an increase in the total number density of ISSC formation can be seen for increasing NaCl. Apparently, a single calcium ion is replaced by more than one sodium ion. In figure 5.4b the charge density in the ISSC is shown. At first, the charge density decreases slightly by 12% when NaCl increased from 0.0 M to 0.2 M. This can be explained by the lower valency of Na^+ compared to Ca^{2+}. However, when the NaCl concentration is further increased to 0.5 M and 0.7 M, the charge density increases by 28% and 19% despite the lower valency of Na^+. Note that repellent lateral ion-ion correlations between cations on the surface are weaker for sodium ions. This might also play a role in the extra sodium adsorption. The total ion density and total charge density against z can be found in appendix B.1.

Figure 5.3a and 5.3b show that the absolute amount of Ca^{2+} OSSC decrease is comparable to the absolute amount of Na^+ OSSC increase, between 0.08 and 0.1 nm^{-3} for each step of increasing NaCl. This agrees with the total number density of OSSC in figure 5.4a, which is the same for each concentration. Because Na^+ has a lower valency than Ca^{2+}, the total charge density of OSSC decreases as shown in figure 5.4a. The decrease in OSSC charge density and the increase in ISSC charge density balance each other, leading to a similar charge inversion magnitude as was shown in figure 5.1.

Comparing figures 5.5 and 5.4b, it is visible that chloride has a negligible effect on the discussion above, where it was explained that the ISSC and OSSC's contribution to the CI magnitude balance each other. In figure 5.3c it is visible that the amount of chloride increases for increasing concentration.

It was mentioned that Bourg and Sposito [19] found increasing charge inversion for increasing ionic strength. They suggest that this is caused by the affinity of the smectite surface for $CaCl^+$ pairs, and the formation of such pairs increases when the ionic strength increases. We did not find a clear affinity for calcium ions, and obvious pairing between calcium and chloride did not occur (see appendix B.2). Note that pairing in MD simulations is known to be difficult to predict [19, 65], which can be a reason for the dissimilarity.

5.2. Electrokinetic Properties

The electroosmotic flow can exhibit flow reversal or a tendency towards FR. Flow reversal is associated with a positive zeta potential (ζ) for a negatively charged amorphous silica interface. Van Der Heyden *et al.* [1] and Semenov *et al.* [12] have shown that the zeta potential of the silica interface in contact with multivalent electrolyte decreases towards (more) negative values when ions of a lower valency are added. This is in line with the findings for charge inversion reduction in electrolyte mixtures discussed in section 5.1. A tendency towards FR is found in our work, although FR is not present. The expected suppression of this tendency towards FR does not occur: the zeta potential for each concentration is the same within uncertainty. This section discusses the electrokinetic properties over time and tries to connect them to the adsorption properties.

5.2.1. Electrokinetic properties over time

The electroosmotic flow velocity, which is the velocity in z-direction in the bulk of the channel, is plotted over time in figure 5.6 for the total duration for which the simulation was performed. The EOF velocity decreases and increases in speed continuously. The mean of the velocity fluctuations does not exhibit flow reversal. It is visible that there is no clear distinction between the magnitude of the electroosmotic flow velocities of each concentration. The last 25 ns of each dataset is used for the production run. More information about the representativeness of this sample can be found in appendix C.1. The standard deviation over the datapoints over time decreases from 1.7 m/s for 0M NaCl to 1.4 m/s for 0.7 M NaCl. This is likely to be caused by the smaller amount of ions present for 0.0 M NaCl.

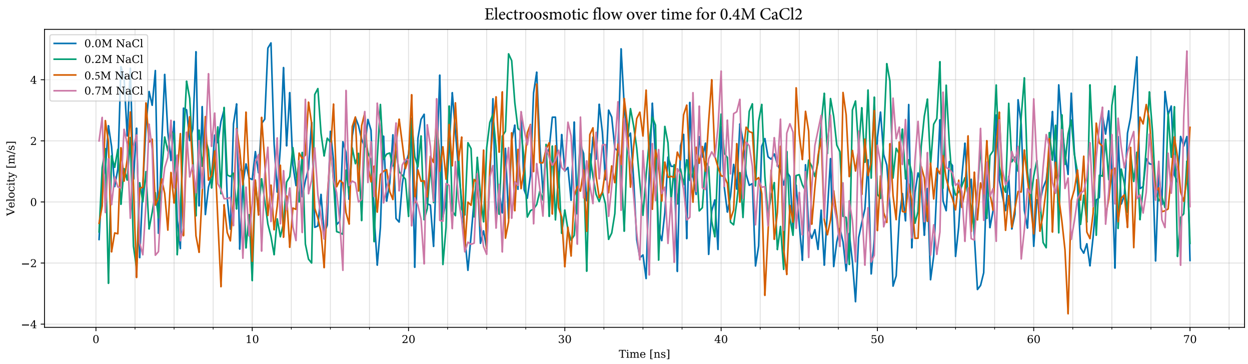

Figure 5.6: The electroosmotic flow velocity over the total time.

Adsorption over time

When ions desorb, they become more mobile. So if they remain in the EDL, they contribute more to the flow velocity. Therefore, the adsorption count of the cations decreases when a cation desorbs, and the velocity in the EDL should become more positive. An inverse correlation between cation adsorption and EOF is thus expected. By plotting the adsorption against the EOF over time for a single simulation, the direct relation between adsorption and velocity can be investigated. The results are shown for a single simulation for 0.0 M and 0.7 M NaCl. The other results can be found in appendix C.2. First, ISSC and OSSC adsorption for the electrolyte with $CaCl_2$ only from figure 5.7 is discussed. Then the adsorption for 0.7 M NaCl is investigated. The adsorption for 0.7 M NaCl is more complex since both Na^{+} and Ca^{2+} are present. First, the ISSC and OSSC adsorption is compared using figure 5.8. Then the difference between Na^{+} and Ca^{2+} adsorption is discussed with figure 5.9. Finally, we try to estimate the contribution of both Na^{+} and Ca^{2+} ISSC and OSSC by looking at figure 5.10.

Figure 5.7 shows the ISSC and OSSC adsorption of Ca^{2+} over time against the EOF for the concentration with 0.0 M NaCl and 0.4 M $CaCl_2$. Opposing peaks are present for ISSC adsorption in figure 5.7a, for example at 61.5, 63.5 and 64.5 nanoseconds. Overall, the ISSC adsorption and the EOF show an inverse correlation. For OSSC adsorption in figure 5.7b opposing peaks are also visible. However, at for example 63.5 and 66.5 nanoseconds an opposing trend is lacking. Overall, the OSSC adsorption shows less inverse correlation with the EOF than ISSC adsorption. It is concluded that for this concentration with no NaCl, the ISSC Ca^{2+} adsorption is dominant for the EOF for NaCl-$CaCl_2$ mixtures.

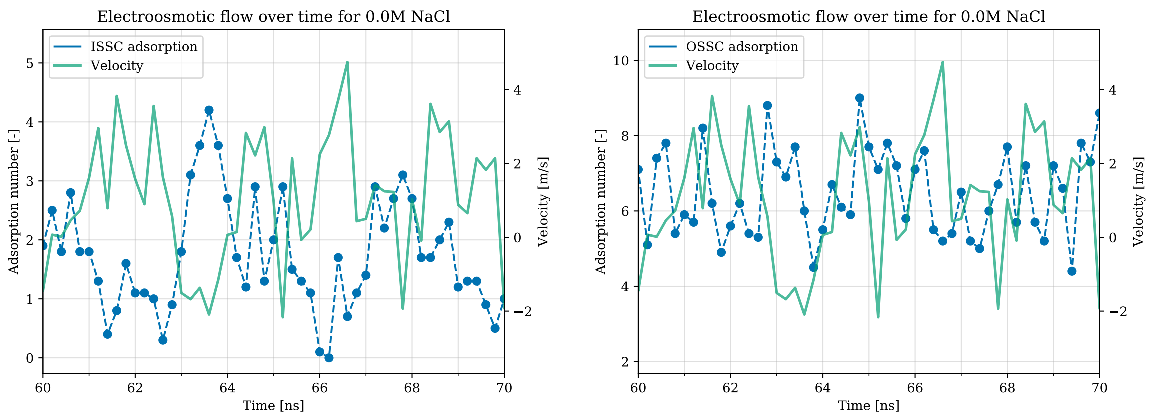

(a) ISSC adsorption and EOF velocity over time.

(b) OSSC adsorption and EOF velocity over time.

Figure 5.7: Velocity against adsorption type over time for 0.0 M NaCl.

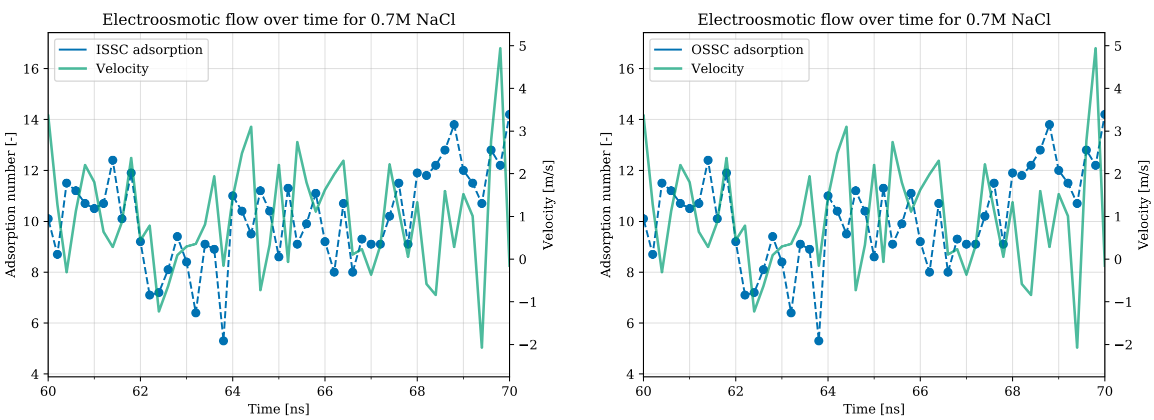

(a) ISSC adsorption and EOF velocity over time.

(b) OSSC adsorption and EOF velocity over time.

Figure 5.8: Velocity against adsorption type over time for 0.7 M NaCl.

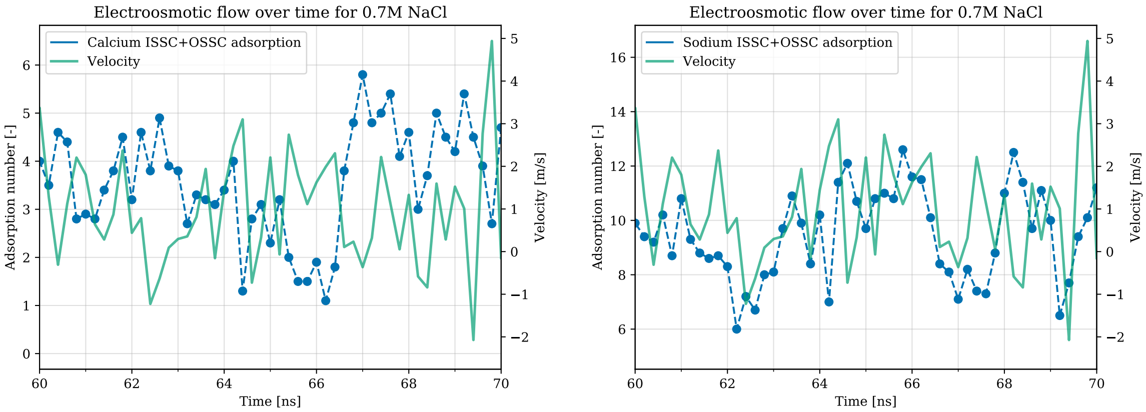

(a) Velocity against calcium adsorption over time. (b) Velocity against sodium adsorption over time.

Figure 5.9: Velocity against ion species for 0.7 M NaCl.

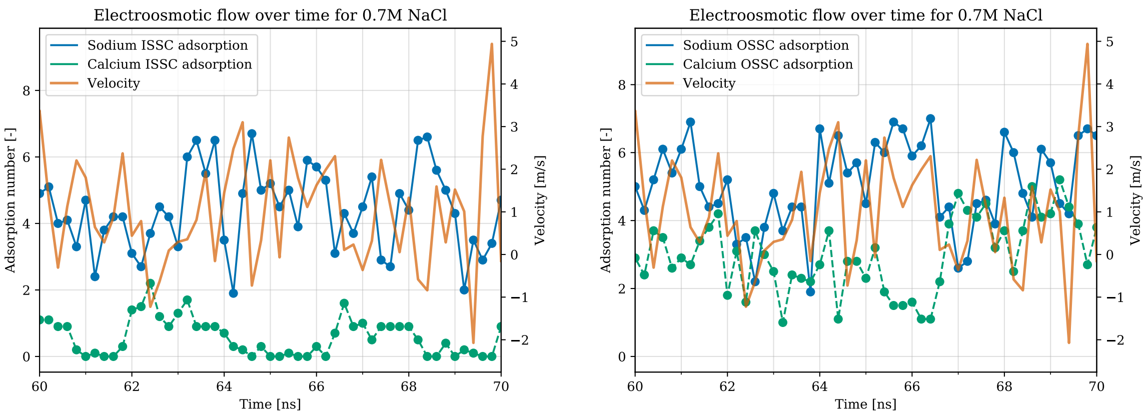

(a) Velocity against sodium and calcium ISSC adsorption over time. (b) Velocity against sodium and calcium OSSC adsorption over time.

Figure 5.10: Velocity against ion adsorption type per species for 0.7 M NaCl.

Figure 5.8 shows the total ISSC and OSSC adsorption over time for 0.7 M NaCl and 0.4 M $CaCl_2$. Figure 5.8a shows many opposing peaks for ISSC adsorption, although the trend is not as strong as for 0.0 M NaCl in figure 5.7a. For example, at 60.5 and 63 nanoseconds, the adsorption peaks do not oppose the EOF peaks. Figure 5.8b shows some opposing peaks for OSSC adsorption, but there are some regions that do not follow this trend, for example between 61.5 and 62.5 nanoseconds. Overall, both ISSC and OSSC seem to have a contribution to the EOF, but it is hard to specify more from this figure.

Figure 5.9 shows the total Na and Ca^{2+} adsorption as ISSC and OSSC against the EOF. Overall, the trend of opposing peaks for Ca^{2+} adsorption in figure 5.9a is more present than for Na^+ in figure 5.9b, so it can be concluded that Ca^{2+} adsorption is more dominant for the EOF than Na^+. Yet, the trend for Na^+ adsorption is not completely lacking.

To get a better insight into the difference between sodium and calcium adsorption, and the total ISSC and OSSC adsorption, the individual Ca^{2+} ISSC and Na^+ ISSC adsorption are plotted in 5.10a and the individual Ca^{2+} OSSC and Na^+ OSSC adsorption are plotted in 5.10b. In figure 5.10a the ISSC adsorption of Na^+ shows some inverse correlation to the

EOF, but it is not as clear as for the Ca^{2+} ISSC for 0.0 M Na^{+} in figure 5.7a. The Ca^{2+} ISSC adsorption fluctuates less over time and no direct correlation is visible. If we compare the total ISSC adsorption in 5.8a to the Na^{+} and Ca^{2+} ISSC in figure 5.10a, it is clear that Na^{+} ISSC formation is responsible for the correlation between ISSC adsorption and EOF. Figure 5.10b shows there are some opposing peaks between Na^{+} OSSC adsorption and the EOF, but the inverse correlation between Ca^{2+} OSSC formation and the EOF is more clear. If we compare the total Ca^{2+} adsorption in 5.9a to Ca^{2+} ISSC and OSSC in figure 5.10a, it is clear that Ca^{2+} OSSC formation causes the correlation between OSSC adsorption and EOF. Finally, it is concluded that Ca^{2+} OSSC adsorption and Na^{+} ISSC adsorption are the main driving factors for the EOF profile.

5.2.2. Average electrokinetic properties

This section presents the average electrokinetic properties over the last 25 ns of each concentration and tries to relate them to the structural properties of the EDL.

Zeta potential

The zeta potential for each concentration is shown in figure 5.11. Similarly to the lack of a trend in the screening profile, there is a lack of trend for the zeta potential. All values are within uncertainty. This is not in line with studies that have found decreasing zeta potential towards more negative values when ions of a lower valency are added to a multivalent solution [1, 12], and also not with studies that found increasing zeta potential for increasing ionic strength [1, 17, 50]. For a discussion on why this could be the case, refer to section 5.3.

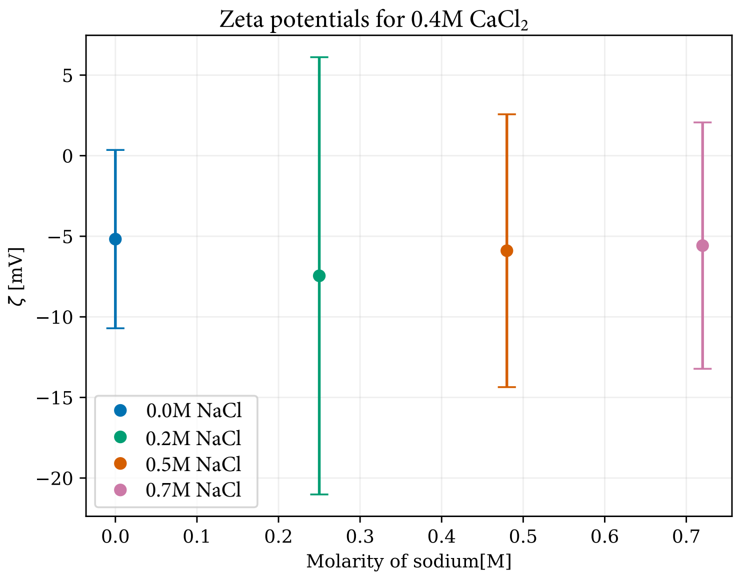

Figure 5.11: The zeta potential for each concentration.

Ion transport diffusion

The ion transport diffusion is shown in figure 5.12. The diffusion coefficients are in line with those calculated by Döpke and Hartkamp [57]. The chloride ions have the highest transport diffusion for each adsorption type. The diffusion coefficient for calcium is smaller than for sodium, so the calcium ions move less. This indicates that calcium adsorbs more strongly than sodium.

The diffusion is similar for all concentrations: any trend that seems to be present is within the error margins which are larger than the figure [57].

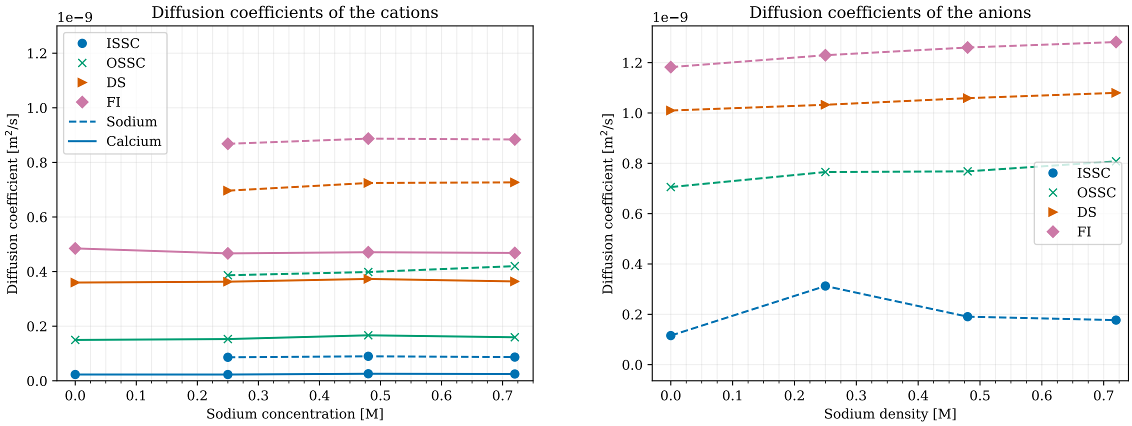

(a) Diffusion coefficient for sodium and calcium ions. (b) Diffusion coefficient for chloride ions.

Figure 5.12: Transport diffusion coefficient for all ion species.

Velocity profile

The velocity profiles of all components for 0.5 M NaCl and 0.4 M $CaCl_2$ are shown in figure 5.13 to illustrate that the water profile is a result of the ion velocities. Figure 5.14 shows the water velocity along the channel. The trend in bulk concentration is not distinct, as was shown in the EOF over time in figure 5.6. The peaks in the diffuse layer decrease by 0.7 m/s for both NaCl concentrations of 0.5 M and 0.7 M. Theoretically, the total amount of adsorbed ISSC, OSSC and DS ions times their transport diffusion coefficient from figure 5.12 would lead to the height of the water velocity peak. For increasing NaCl concentration, the location at which bulk velocity is reached decreases from 2.3 nm for 0.0 M NaCl to 1.9 nm for 0.7 M NaCl. This directly correlates to the width of the chloride peak in the diffuse layer as shown in figure 5.15. This is no surprise, as the width of the diffuse layer is known to decrease with increasing concentration.

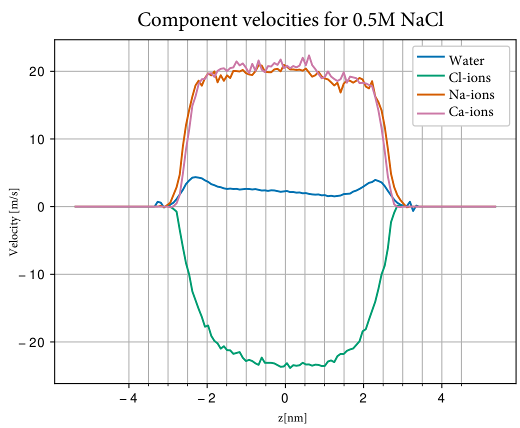

Figure 5.13: The ion velocity and water velocity for 0.5 M NaCl along the channel.

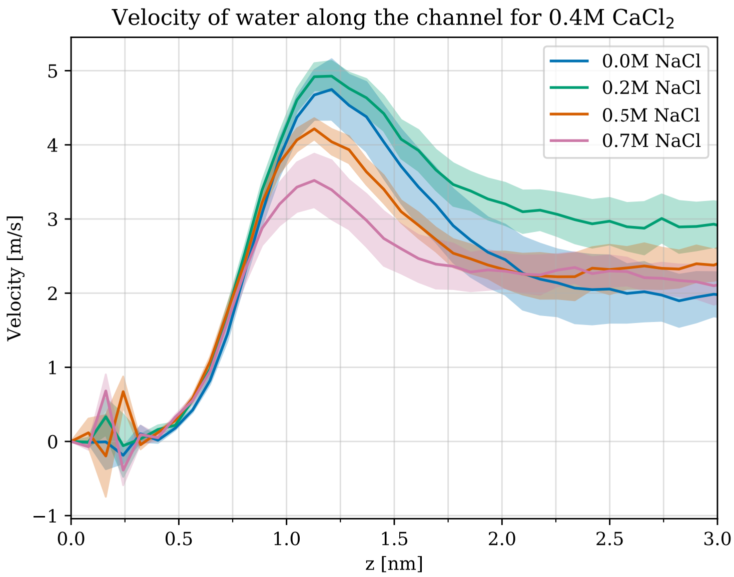

Figure 5.14: The velocity profiles of water along the channel for each concentration.

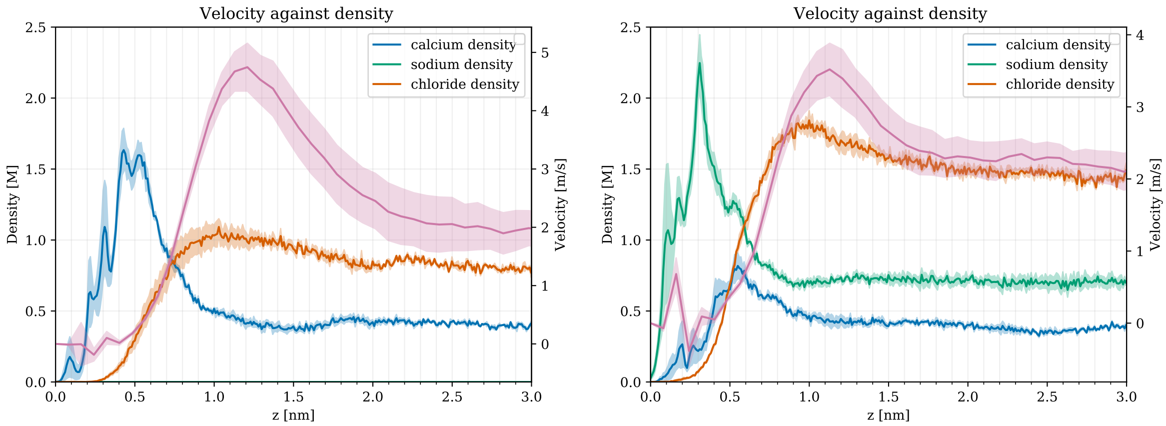

(a) Velocity against ion density for 0.0 M NaCl.

(b) Velocity against ion density for 0.7 M NaCl.

Figure 5.15: Velocity and density profiles.

Shear plane location

The shear plane location is dependent on the zeta potential and the ion density close to the wall. The intersection between the electric potential (calculated with NS-equation) and the zeta potential (calculated using the HS-equation) lies at the theoretical shear plane (see appendix D. When the error of the shear plane location is calculated, the contribution of the error of the density profile is neglected, as it is small in comparison to the error of the zeta potential. Figure 5.16 shows the theoretical shear plane location for each concentration. Comparing these locations to the velocity and the ion density in for example 5.15a and 5.15b it is clear that these locations can not be related to an obvious Stern Layer width. This emphasizes the fact that results obtained from analytical models like Helmholtz-Smoluchowksi (equation 2.13) should be interpreted with caution.

However, the decreasing trend of shear plane location to the wall is in line with the findings by Brown *et al.* [38], who found that Stern Layer thickness decreased for increasing ionic concentration. In our case, a decrease of Stern Layer width can also be explained by the replacement of calcium ions by sodium ions, which have a weaker hydration shell and can move closer to the wall [54]. This is also visible in the screening profile in figure 5.1.

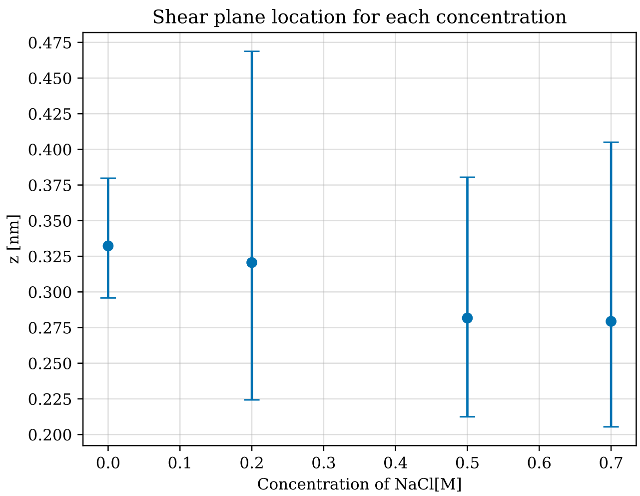

Figure 5.16: The theoretical shear plane location to the wall for each concentration.

5.3. Results in Context of Existing Literature

Table 5.1 contains information on the studied mixtures by Van Der Heyden *et al.* [1], Szymanek *et al.* [17], Bourg and Sposito [19], Thanh *et al.* [50] and this work. For all studies, except for Bourg and Sposito, amorphous silica was the surface material although different ions are used. The work by Bourg and Sposito is still included because the same aqueous ionic mixtures with similar concentrations were studied with MD. The differences between Bourg and Sposito [19] and our work in structural properties originate from the different surface material: they used smectite instead of amorphous silica, which leads to different ISSC and OSSC adsorption than in our systems. This was discussed in 5.1. This section also includes the values for the experiments by Van der Heyden *et al.* for a single divalent $CaCl_2$ electrolyte, as it measured the critical concentration for $CaCl_2$. The system concentrations and values for ζ that were measured are compared, placing our findings in the context of previous work.

Figure 5.17 shows the ionic strengths of different research. Note that the ionic strengths of this work and Bourg and Sposito, both using MD simulations, are generally higher than the experimental work. The divalent system studied by Van der Heyden *et al.* also accesses higher ionic strengths, which is a big advantage of streaming current experiments over other experimental methods.

Table 5.1: Studies that have researched electrokinetic properties of mixtures. Values for Semenov *et al.* [12] were not published.

Source	Method	Mono	Multi	Anion	Surface
Van Der Heyden *et al.* [1]	SC	K^+	CoSep	Cl^-	Amorphous silica
Van Der Heyden *et al.* [1]	SC	none	Ca^{2+}	Cl^-	Amorphous silica
Szymanek *et al.* [17]	Electrophoresis	K^+	Ca^{2+}	Cl-	Amorphous silica
Thanh *et al.* [50]	Electrophoresis	Na^+	Ca^{2+}	SO_4^-,Cl^-	Amorphous silica
This work	MD (Electroosmosis)	Na^+	Ca^{2+}	Cl^-	Amorphous silica
Bourg and Sposito [19]	MD	Na^+	Ca^{2+}	Cl^-	Smectite

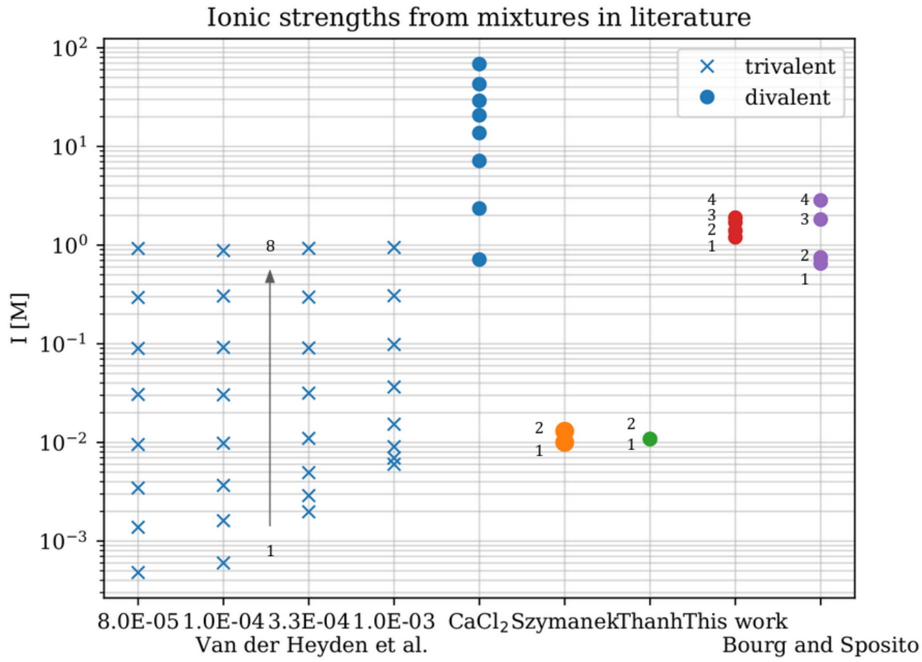

Figure 5.17: The ionic strengths of previous research and this work. 'x' denotes trivalent mixtures, a dot denotes divalent mixtures. The datapoints can be found in table 5.1. Data taken from [1, 17, 50].

The monovalent concentrations against the multivalent concentrations from literature are plotted in figure 5.18. There is 1 point for the divalent electrolyte by Van der Heyden *et al.* that coincides with our simulations, namely at a $CaCl_2$ concentration of 0.4 M. This is the point at which Van der Heyden *et al.* found CI for divalent electrolytes, also indicated by the red vertical line. The blue vertical line indicates CI for trivalent CoSep electrolyte as found by Van der Heyden *et al.* Both our work and the work of Van der Heyden *et al.* regarding mixtures start at a point where CI occurs. This was done on purpose as our research tried to mimic the trivalent-monovalent mixture but with divalent instead of trivalent electrolyte. Note that the monovalent concentration has to be varied against a set multivalent concentration, as this was done in all research that found CI reduction and FR suppression [1, 12–14].

Szymanek *et al.* and Thanh *et al.* did not find CI due to the low ionic strengths in their systems, and instead of varying the multivalent concentration, they vary the monovalent

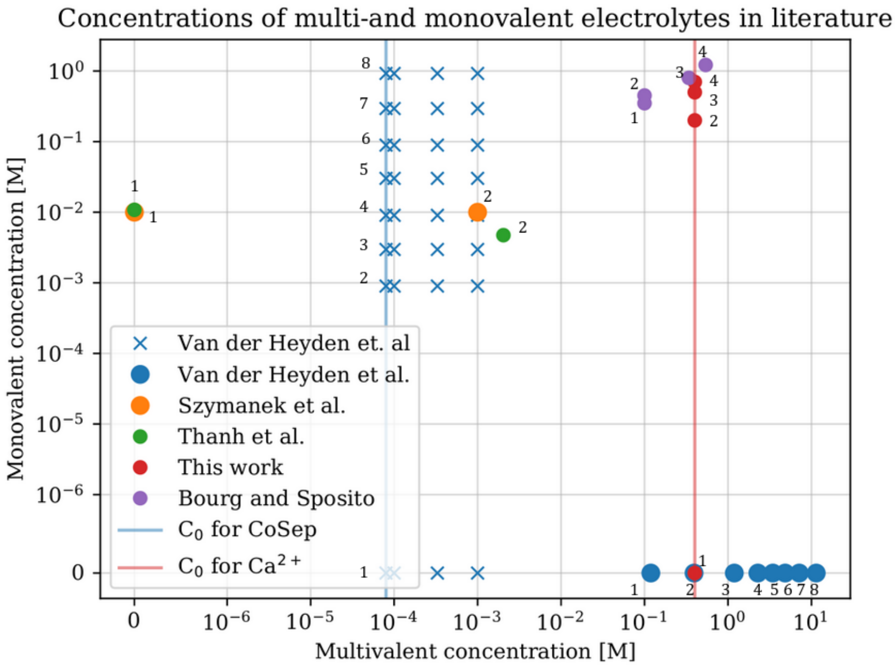

Figure 5.18: The concentration of multivalent against monovalent components of previous literature and this work. 'x' denotes trivalent mixtures, a dot denotes divalent mixtures. The datapoints can be found in table 5.1. Data taken from [1, 17, 50].

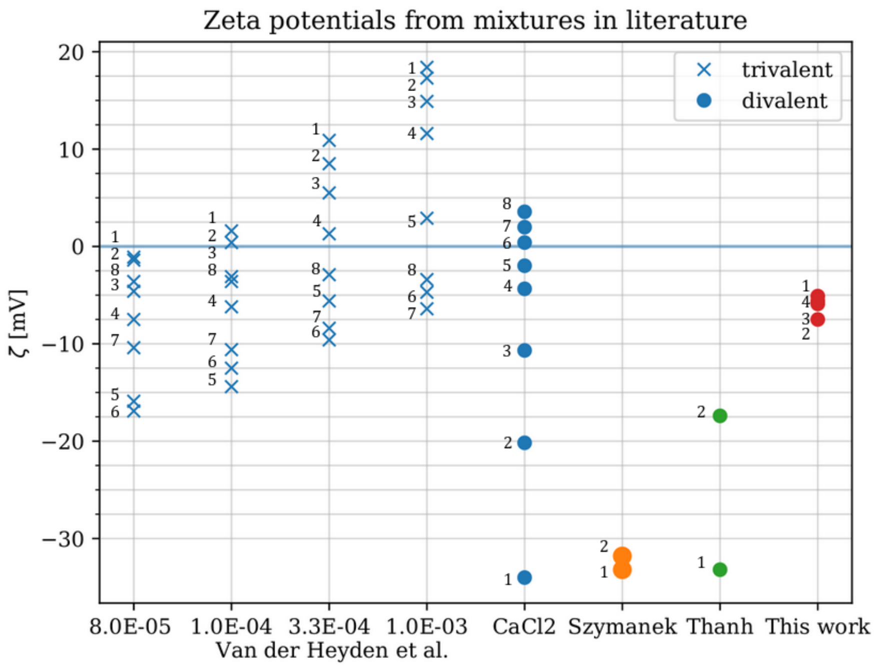

Figure 5.19: The zeta potential for different mixtures from previous literature and this work. 'x' denotes trivalent mixtures, a dot denotes divalent mixtures. Flow reversal occurs for positive values above the line at ζ=0. The datapoints can be found in table 5.1. Data taken from [1, 17, 50]

concentration. Consequently, ζ becomes less negative, so the tendency towards FR increases. This is visualised in figure 5.19, which shows all zeta potentials for the data points from figure 5.18. A reason for the increase of tendency towards FR could be that Szymanek *et al.* and Thanh *et al.* probe concentrations which are far below the flow reversal regime, so electrostatic interactions between the surface and the ions are more dominant than for example ion-ion correlations, causing the expected increase in surface screening.

The data of Van der Heyden *et al.* shows that the zeta potential first moves away from FR, after which it moves towards FR again. ζ for point 8 is comparable to point 1 and 2 for the lowest multivalent concentration. This can also be directly seen from figure 5.20. Two regimes can be distinguished: one that shows CI reduction when monovalent ions are initially added, and one that shows CI enhancement when more monovalent ions are added.

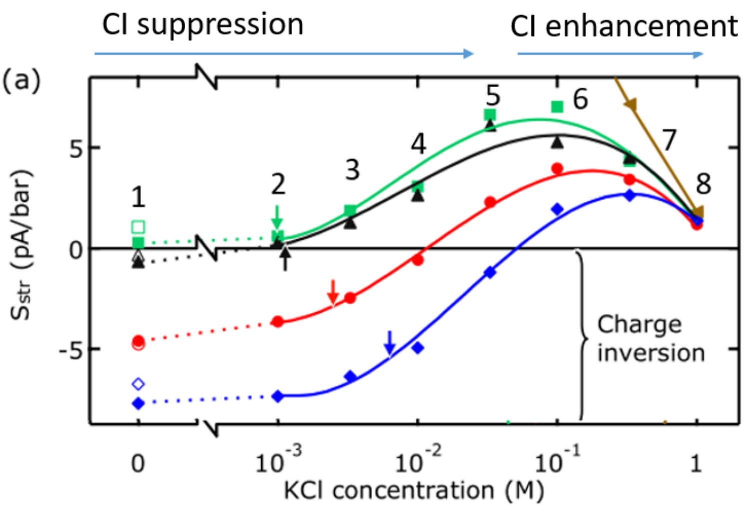

Figure 5.20: The streaming conductance that Van Der Heyden *et al.* [1] found for mixtures of $CoSepCl_3$ and KCl. Figure adapted from [1].

For our work, ζ for all 4 concentrations is comparable. This makes it difficult to conclude anything on which mechanisms cause the CI decrease and FR suppression. However, it is possible that the reason the points are comparable is in line with why for example points 1,2,3 and 8 for Van der Heyden's lowest starting concentration are similar to each other.

It can be hypothesised that the increasing FR tendency between, for example, point 6 and 8 for the mixtures in the work by Van der Heyden *et al*, originates from ion competition for ISSC adsorption. In line with our work, multiple sodium ions would then replace single calcium ions. The suppression of FR for smaller additions of monovalent ions (the other regime) would mean that single multivalent ions are replaced by single monovalent ions, also as ISSC, decreasing the CI magnitude. Unfortunately, it is hard to conclude whether this hypothesis is correct because suppression of FR was not replicated by our work. It is also unknown what the exact mechanisms are behind trivalent and divalent adsorption and how they are dissimilar: while the critical concentration of $CoSepCl_3$ lies in the regime of

FR suppression, the critical concentration of divalent electrolyte may lie elsewhere on the curve in figure 5.20. If the concentrations for NaCl-$CaCl_2$ mixtures that we simulated lies between the CI suppression and CI enhancement regime, it would not be surprising that the screening function did not vary.

5.4. Discussion

Several assumptions have been made that might affect the results found in this thesis. They are discussed below.

Surface effects

Figure 5.21 shows the calcium ion density on the left side of the channel for each individual simulation of 0.5 M NaCl and 0.4 M $CaCl_2$. The width and height of the adsorption peak vary. This explains why the electrokinetic properties of individual simulations of the same concentration vary as well as shown in 5.22. The variations are caused by the variation of the surface because each wall of each simulation has a different deprotonation configuration. According to Döpke *et al.* [18], the protrusion of these deprotonation sites affects preferential adsorption of ions as ISSC and OSSC: the hydration shell of Ca^{2+}, which is stronger than that of Na^+, can cause steric hindrance, preventing calcium ions to adsorb. In this thesis, it is assumed that averaging 6 wall configurations (left and right for 3 different simulations) results in a representative amorphous silica surface structure. It could be possible that more data is needed to obtain a physically representative amorphous silica surface, more so because the starting block of amorphous silica is the same for each simulation.

Discretization of the surface charge

The bare surface charge is chosen such that it matches a pH of 7.5 for the simulated bulk concentrations. It was argued that it was desirable to have the same deprotonation number for each concentration to be able to compare the concentrations without surface effects distorting the results. It was discussed that it is not known how exactly the bare surface charge for aqueous ionic mixtures relates to the values for single electrolytes in figure 3.5. The deprotonation number for all simulated concentrations is 8. Thus if the sodium proportion increases, the bare surface charge decreases with an estimated value of 15 mC/m^2 when the lines are interpolated in such a way that the contribution of ion species is proportional to their concentration. This effect is not accounted for in our simulations. This might result in an overestimation of charge inversion for concentrations with a higher sodium proportion. This is important, as it might be a reason why CI reduction and FR suppression was not found in this work. Moreover, the discretization of deprotonation sites also leads to a maximum deviation of 7 mC/m^2 in the obtained bare surface charge compared to the desired surface.

Forcefield parameters

Döpke and Hartkamp have found that scaling the interaction between calcium and surface atoms improves the prediction of calcium adsorption on the surface. This is not done for chloride and sodium atoms. Furthermore, general mixing rules are applied for interatomic interactions between calcium and sodium. ISSC and OSSC adsorption in MD simulations are very sensitive to these parameters. Ion competition between calcium and sodium might also be affected. If the interactions are not correct, this will lead to different ISSC and OSSC adsorption behaviour. This can cause big deviations in the observed screening profiles.

The electrokinetic behaviour will also strongly differ as it was shown in section 5.2 that the EOF is very sensitive to the adsorption behaviour in the EDL.

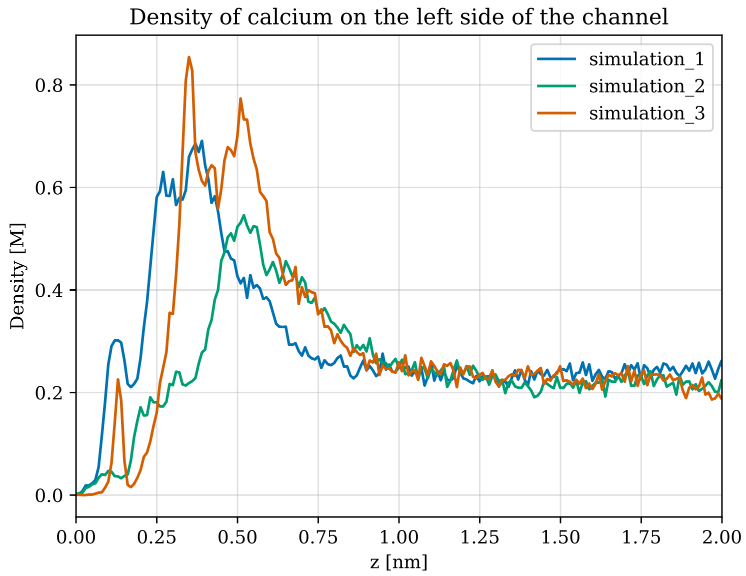

Figure 5.21: The density profile on the left side for individual simulations of 0.2 M NaCl.

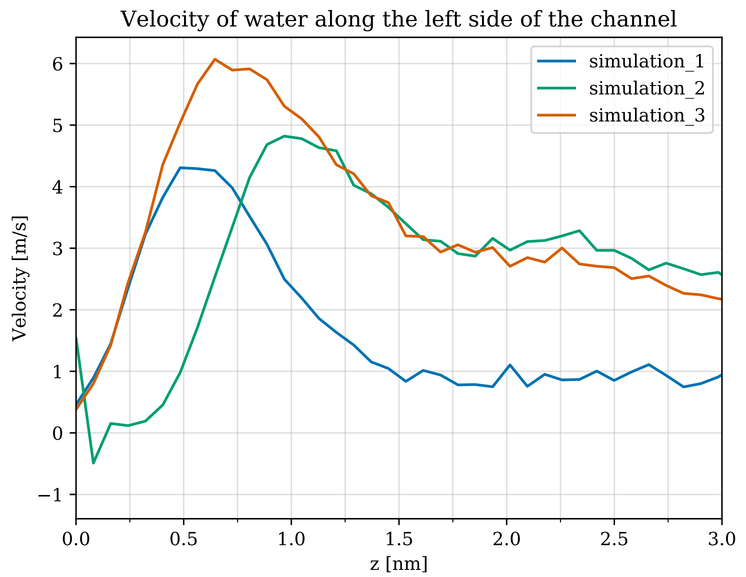

Figure 5.22: The velocity profile on the left side for individual simulations of 0.0 M NaCl.

6 Conclusion

The hypothesis of this thesis was that adding sodium chloride to a calcium chloride mixture leads to a decrease of charge inversion, which also reduces the flow reversal effect. Using molecular dynamics simulations, a system with an amorphous silica surface was studied, consisting of 0.4 M $CaCl_2$ and a varying concentration of NaCl (0 - 0.7 M). We found that the variation of charge inversion and electroosmotic flow velocity is negligible. This gives us the answer to the main research question:

> **Can the transport of a calcium chloride solution be controlled by adding sodium chloride?**

This is not the case for the system that we studied. By answering the subquestions we provide insight into why the results were not as expected.

> **How does adding sodium ions to a calcium chloride mixture affect the charge inversion and flow reversal?**

Screening and velocity profiles show that the addition of sodium to the system does not lead to a different charge inversion magnitude. Although flow reversal was not found, the flow reversal tendency was present and was not suppressed by the addition of sodium.

> **How do different ion types adsorb at the surface?**

Although the charge inversion magnitude and electroosmotic flow did not significantly change, our results show that the adsorption of calcium and sodium in the EDL varied for different concentrations. The total ISSC adsorption increases, so one calcium ion is outcompeted by multiple sodium ions, whereas total OSSC adsorption remains the same. Therefore, the ISSC's contribution to charge inversion increases. The OSSC's contribution to charge inversion on the other hand decreases due to the lower valency of sodium. These effects of ISSC and OSSC adsorption on the charge inversion balance each other, leading to the same charge inversion magnitude.

How do electrokinetic properties relate to the EDL structure for electrolyte mixtures?

Firstly, it was shown that flow reversal does not occur concurrently with charge inversion, which opposes the common assumption that these phenomena always occur together. We found that the EOF is sensitive to the dynamic adsorption of the ions in the EDL. It was shown that for $CaCl_2$, ISSC adsorption has more impact on the EOF than OSSC adsorption. For higher NaCl concentrations, Na^+ ISSC adsorption and Ca^{2+} OSSC adsorption show a bigger contribution.

Now that the research questions have been answered, the limitations of this research are summarised. The sensitivity of the EOF to the adsorption in the EDL emphasises the need for careful tuning of the force field parameters between the surface and the ions, which is currently only done for calcium. Also, the bare surface charge is a near approximation of its real value due to the lack of titration data for mixtures and discretization of charges on the surface. Another limitation of our MD simulations is that the amount of data used might distort the results. A longer production run and more surface configurations might lead to more realistic data.

Nonetheless, this research is the first that uses MD simulations to study the effect of adding monovalent ions to a multivalent solution for an amorphous silica surface on both structural properties of the EDL and electrokinetic properties. CI and FR were not significantly altered by adding sodium ions. This disproves the idea that transport of multivalent electrolytes can be controlled by adding monovalent ions for systems comparable to ours in terms of valency, concentration and material. Although the results cannot be directly applied to the transport control in the design of nanofluidic devices, the results of this thesis could still be used to improve models that predict structural and electrokinetic properties for aqueous ionic mixtures.

6.1. Recommendations

To further investigate the charge inversion and flow reversal in electrolyte mixtures, some research recommendations are described.

Performing SC experiments for divalent-monovalent mixtures

Van Der Heyden *et al.* [1] has found a curve for charge inversion against addition of monovalent ions to trivalent electrolytes. It is unknown what this curve looks like for divalent-monovalent mixtures. If the SC experiments would be performed for divalent-monovalent mixtures, it would be clear whether the regimes of CI decrease and increase are the same as for trivalent-monovalent mixtures. It would then be possible to place our results within the context of the work by van Der Heyden *et al.*, and determine if the results we found are also applicable to their findings.

Varying the hydration strength of ions

To determine the contribution of hydration strength of the ions on ion competition and charge inversion, the simulations in this work can be repeated with divalent and monovalent ions with a different hydration strength. For example, potassium has a lower hydration strength than sodium, so more ISSC formation would be expected. Note that the size of different ions may also vary.

Increasing CI of the starting concentration

In this thesis, the zeta potential of each concentration is similar, so the decreasing CI was not found when monovalent ions were added. This makes it impossible to conclude what adsorption phenomena in the EDL contribute to CI reduction and FR suppression. Previous studies found that the higher the initial charge inversion (the more flow reversal) for single trivalent electrolytes, the more pronounced the charge inversion reduction (and FR suppression) becomes when monovalent salt is added to the solution. Assuming that this is also the case for divalent-monovalent mixtures, it is suggested that the initial CI magnitude of the single $CaCl_2$ electrolyte is increased. This can be done by increasing the concentration and consequently the bare surface charge of the simulations. This way, the zeta potential for $CaCl_2$ in figure 5.19 will move upwards towards more positive values, whereas the zeta potential of the mixtures to which monovalent ions are added will be lower. If this is the case, it would be possible to research what structural properties within the EDL contribute to the CI reduction and FR suppression.

Varying the bare surface charge

In this thesis, it is assumed that the pH of a solution can be simulated by obtaining the corresponding bare surface charge in the system. The presence of hydroxonium and hydroxide ions is not simulated. Exploring other pH-values with MD simulations could indicate how accurate this assumption is by comparing the adsorption to the ion uptake for different pH-values from literature [33]. It is also possible to validate the force field by simulating the isoelectric point ($\zeta = 0$) of other pH-values with MD simulations. If a range of pH-values can accurately be simulated using MD simulations, this would open a new range of research possibilities. For example, the effect of pH-value specifically on ion competition has been experimentally studied [15, 17, 29], and MD simulations can complement these studies by uncovering the ion competition mechanisms on an atomic level. Finally, if the results from MD agree with experimental values, it would also be possible to develop an accurate surface complexation model, which gives insight into how species exactly adsorb on the interface.

Bibliography

[1] F. H. Van Der Heyden, D. Stein, K. Besteman, S. G. Lemay, and C. Dekker, *Charge inversion at high ionic strength studied by streaming currents,* Physical Review Letters **96**, 1 (2006).

[2] W. E. Marlatt, M. Budyko, and D. Miller, *Climate and life,* Journal of Range Management **28**, 160 (1975).

[3] I. Edelman and J. Leibman, *Anatomy of body water and electrolytes,* The American journal of medicine **27**, 256 (1959).

[4] S. Prakash and J. Yeom, *Nanofluidics and Microfluidics: Systems and Applications* (Elsevier, 2014).

[5] F. Heyden, Bonthuis, D.J., D. Stein, C. Meyer, and C. Dekker, *Power generation by pressure-driven transport of ions in nanofluidic channels,* Nano Letters , 1022 (2007).

[6] C. Dekker, *Solid-state nanopores,* Nature Nanotechnology , 209 (2007).

[7] N. Ravindra, V. R. Mehta, and S. Shet, *Silicon nanoelectronics and beyond: An overview and recent developments,* JOM **57**, 16 (2005).

[8] R. Sivakumarasamy and R. Hartkamp, *Selective layer-free blood serum ionogram based on ion-specific interactions with a nanotransistor,* Nature Materials , 464 (2018).

[9] R. S. Leung, K., *Salt permeation and exclusion in hydroxylated and functionalized silica pores,* Physical Review Letters **96**, 9 (2006).

[10] M. Caglar and U. F. Keyser, *Ionic and molecular transport in aqueous solution through 2d and layered nanoporous membranes,* Journal of Physics D: Applied Physics (2021).

[11] T. Austad, A. RezaeiDoust, T. Puntervold, *et al.*, *Chemical mechanism of low salinity water flooding in sandstone reservoirs,* in *SPE improved oil recovery symposium* (Society of Petroleum Engineers, 2010).

[12] I. Semenov, S. Raafatnia, M. Sega, V. Lobaskin, C. Holm, and F. Kremer, *Electrophoretic mobility and charge inversion of a colloidal particle studied by single-colloid electrophoresis and molecular dynamics simulations,* Physical Review E - Statistical, Nonlinear, and Soft Matter Physics **87**, 1 (2013).

[13] Y. Wang, R. Wang, T. Gao, and G. Yang, *The mixing counterion effect on DNA compaction and charge neutralization at low ionic strength,* Polymers **10**, 38 (2018).

[14] O. Lenz and C. Holm, *Simulation of charge reversal in salty environments: Giant overcharging?* European Physical Journal E **26**, 191 (2008), arXiv:0711.0199 .

[15] M. Kosmulski, *Co-adsorption of mono- and multivalent ions on silica and alumina,* Berichte der Bunsengesellschaft/Physical Chemistry Chemical Physics **98**, 1062 (1994).

[16] S. S. Lee, C. Park, N. C. Sturchio, and P. Fenter, *Nonclassical Behavior in Competitive Ion Adsorption at a Charged Solid-Water Interface,* Journal of Physical Chemistry Letters **11**, 4029 (2020).

[17] K. Szymanek, R. Charmas, and W. Piasecki, *Investigations of mechanism of Ca2+ adsorption on silica and alumina based on Ca-ISE monitoring, potentiometric titration, electrokinetic measurements and surface complexation modeling,* Adsorption (2020), 10.1007/s10450-020-00280-x.

[18] M. F. Döpke, J. Lützenkirchen, O. A. Moultos, B. Siboulet, J. F. Dufrêche, J. T. Padding, and R. Hartkamp, *Preferential Adsorption in Mixed Electrolytes Confined by Charged Amorphous Silica,* Journal of Physical Chemistry C **123**, 16711 (2019).

[19] I. C. Bourg and G. Sposito, *Molecular dynamics simulations of the electrical double layer on smectite surfaces contacting concentrated mixed electrolyte (NaCl-CaCl2) solutions,* Journal of Colloid and Interface Science **360**, 701 (2011).

[20] S. J. Brugman, B. L. Werkhoven, E. R. Townsend, P. Accordini, R. van Roij, and E. Vlieg, *Monovalent – divalent cation competition at the muscovite mica surface: Experiment and theory,* Journal of Colloid and Interface Science **559**, 291 (2020).

[21] A. Markesteijn, R. Hartkamp, S. Luding, and J. Westerweel, *A comparison of the value of viscosity for several water models using poiseuille flow in a nano-channel,* The Journal of chemical physics **136**, 134104 (2012).

[22] R. Qiao and N. R. Aluru, *Charge inversion and flow reversal in a nanochannel electro-osmotic flow,* Physical Review Letters **92**, 1 (2004).

[23] R. B. Schoch, J. Han, and P. Renaud, *Transport phenomena in nanofluidics,* Reviews of Modern Physics **80**, 839 (2008).

[24] L. Henke, N. Nagy, and U. J. Krull, *An AFM determination of the effects on surface roughness caused by cleaning of fused silica and glass substrates in the process of optical biosensor preparation,* Biosensors and Bioelectronics **17**, 547 (2002).

[25] B. Siboulet, S. Hocine, R. Hartkamp, and J. F. Dufrêche, *Scrutinizing Electro-Osmosis and Surface Conductivity with Molecular Dynamics,* Journal of Physical Chemistry C **121**, 6756 (2017).

[26] I. C. Bourg, S. S. Lee, P. Fenter, and C. Tournassat, *Stern Layer Structure and Energetics at Mica-Water Interfaces,* Journal of Physical Chemistry C **121**, 9402 (2017).

[27] J. Rosenqvist, *Surface chemistry of Al and Si (hydr) oxides, with emphasis on nano-sized gibbsite (α-Al (OH) 3),* Ph.D. thesis (2002).

[28] J. Lützenkirchen, T. Preočanin, D. Kovačević, V. Tomišić, L. Lövgren, and N. Kallay, *Potentiometric titrations as a tool for surface charge determination,* Croatica chemica acta **85**, 391 (2012).

[29] W. Janusz, J. Patkowski, and S. Chibowski, *Competitive adsorption of Ca2+ and Zn(II) ions at monodispersed SiO2/electrolyte solution interface,* Journal of Colloid and Interface Science **266**, 259 (2003).

[30] B. Werkhoven, *Static and dynamic solid-water interfaces.*

[31] N. Sahai and D. A. Sverjensky, *GEOSURF: A computer program for modeling adsorption on mineral surfaces from aqueous solution,* Computers and Geosciences **24**, 853 (1998).

[32] T. Hiemstra and W. H. Van Riemsdijk, *A surface structural approach to ion adsorption: The charge distribution (CD) model,* Journal of Colloid and Interface Science **179**, 488 (1996).

[33] M. K. Ridley, M. L. MacHesky, D. J. Wesolowski, and D. A. Palmer, *Calcium adsorption at the rutile-water interface: A potentiometric study in NaCl media to 250°C,* Geochimica et Cosmochimica Acta **63**, 3087 (1999).

[34] K.-C. Chang, Y.-W. Chiang, C.-H. Yang, and J.-W. Liou, *Atomic force microscopy in biology and biomedicine,* Tzu Chi Medical Journal **24**, 162 (2012).

[35] M. Ricci, P. Spijker, and K. Voïtchovsky, *Water-induced correlation between single ions imaged at the solid–liquid interface,* Nature communications **5**, 1 (2014).

[36] M. Ricci, W. Trewby, C. Cafolla, and K. Voïtchovsky, *Direct observation of the dynamics of single metal ions at the interface with solids in aqueous solutions,* Scientific reports **7**, 1 (2017).

[37] M. Ricci, P. Spijker, F. Stellacci, J.-F. Molinari, and K. Voïtchovsky, *Direct visualization of single ions in the stern layer of calcite,* Langmuir **29**, 2207 (2013).

[38] M. A. Brown, A. Goel, and Z. Abbas, *Effect of Electrolyte Concentration on the Stern Layer Thickness at a Charged Interface,* Angewandte Chemie - International Edition **55**, 3790 (2016).

[39] T. A. Gmur, A. Goel, and M. A. Brown, *Quantifying specific ion effects on the surface potential and charge density at silica nanoparticle–aqueous electrolyte interfaces,* The Journal of Physical Chemistry C **120**, 16617 (2016).

[40] R. Hartkamp, B. Siboulet, J. F. Dufrêche, and B. Coasne, *Ion-specific adsorption and electroosmosis in charged amorphous porous silica,* Physical Chemistry Chemical Physics **17**, 24683 (2015).

[41] R. Qiao and N. R. Aluru, *Ion concentrations and velocity profiles in nanochannel electroosmotic flows,* Journal of Chemical Physics **118**, 4692 (2003).

[42] Y. Qiu and Y. Chen, *Counterions and water molecules in charged silicon nanochannels: the influence of surface charge discreteness,* Molecular Simulation **41**, 1187 (2015).

[43] A. Travesset and D. Vaknin, *Bjerrum pairing correlations at charged interfaces,* Europhysics Letters **74**, 181 (2006).

[44] L. Xiang, G. Zhao, D. Zhang, and Y. Chen, *Exploring charge inversion in electrolyte mixtures of trivalent and monovalent ions,* in *2013 International Conference on Manipulation, Manufacturing and Measurement on the Nanoscale* (2013) pp. 283–286.

[45] J. Faraudo and A. Travesset, *The many origins of charge inversion in electrolyte solutions: Effects of discrete interfacial charges,* Journal of Physical Chemistry C **111**, 987 (2007).

[46] B. I. Shklovskii, *Screening of a macroion by multivalent ions: Correlation-induced inversion of charge,* Physical Review E - Statistical Physics, Plasmas, Fluids, and Related Interdisciplinary Topics **60**, 5802 (1999).

[47] C. D. Lorenz and A. Travesset, *Charge inversion of divalent ionic solutions in silica channels,* Physical Review E - Statistical, Nonlinear, and Soft Matter Physics **75**, 2 (2007).

[48] A. Schlaich, E. W. Knapp, and R. R. Netz, *Water dielectric effects in planar confinement,* Physical review letters **117**, 048001 (2016).

[49] A. T. Celebi, B. Cetin, and A. Beskok, *Molecular and Continuum Perspectives on Intermediate and Flow Reversal Regimes in Electroosmotic Transport,* Journal of Physical Chemistry C (2019), 10.1021/acs.jpcc.9b02432.

[50] L. D. Thanh, R. Sprik, and X. C. Nguyen, *Zeta potential of porous rocks in contact with mixtures of monovalent and divalent electrolytes,* Geophysical Prospecting **67**, 1354 (2019).

[51] S. Prakash, H. A. Zambrano, K. K. Rangharajan, E. Rosenthal-Kim, N. Vasquez, and A. T. Conlisk, *Electrokinetic transport of monovalent and divalent cations in silica nanochannels,* Microfluidics and Nanofluidics **20**, 1 (2016).

[52] J. J. López-García, J. Horno, and C. Grosse, *Numerical solution of the electrokinetic equations for multi-ionic electrolytes including different ionic size related effects,* Micromachines **9** (2018), 10.3390/mi9120647.

[53] A. Revil, *Pervasive pressure solution transfer in a quartz sand,* Journal of Geophysical Research: Solid Earth **106**, 8665 (2001).

[54] A. H. Jalil and U. Pyell, *Quantification of Zeta-Potential and Electrokinetic Surface Charge Density for Colloidal Silica Nanoparticles Dependent on Type and Concentration of the Counterion: Probing the Outer Helmholtz Plane,* Journal of Physical Chemistry C **122**, 4437 (2018).

[55] S. Li, P. Leroy, F. Heberling, N. Devau, D. Jougnot, and C. Chiaberge, *Influence of surface conductivity on the apparent zeta potential of calcite,* Journal of Colloid and Interface Science **468**, 262 (2016).

[56] R. Hartkamp, A. L. Biance, L. Fu, J. F. Dufrêche, O. Bonhomme, and L. Joly, *Measuring surface charge: Why experimental characterization and molecular modeling should be coupled,* Current Opinion in Colloid and Interface Science **37**, 101 (2018), arXiv:1808.08799 .

[57] M. F. Döpke and R. Hartkamp, *The importance of specifically adsorbed ions for electrokinetic phenomena: Bridging the gap between experiments and md simulations,* The Journal of Chemical Physics **154**, 094701 (2021).

[58] F. S. Emami, V. Puddu, R. J. Berry, V. Varshney, S. V. Patwardhan, C. C. Perry, and H. Heinz, *Force field and a surface model database for silica to simulate interfacial properties in atomic resolution,* Chemistry of Materials **26**, 2647 (2014).

[59] I. Zeron, J. Abascal, and C. Vega, *A force field of li+, na+, k+, mg2+, ca2+, cl-, and so 4 2- in aqueous solution based on the tip4p/2005 water model and scaled charges for the ions,* The Journal of chemical physics **151**, 134504 (2019).

[60] I.-C. Yeh and M. L. Berkowitz, *Ewald summation for systems with slab geometry,* The Journal of chemical physics **111**, 3155 (1999).

[61] I. M. Zeron, J. L. Abascal, and C. Vega, *A force field of Li+, Na+, K+, Mg2+, Ca2+, Cl-, and S O 4 2 - In aqueous solution based on the TIP4P/2005 water model and scaled charges for the ions,* Journal of Chemical Physics **151** (2019), 10.1063/1.5121392.

[62] M. Laliberte and W. E. Cooper, *Model for calculating the density of aqueous electrolyte solutions,* Journal of Chemical & Engineering Data **49**, 1141 (2004).

[63] G. E. Christidis, A. E. Blum, and D. Eberl, *Influence of layer charge and charge distribution of smectites on the flow behaviour and swelling of bentonites,* Applied Clay Science **34**, 125 (2006).

[64] T. Underwood, V. Erastova, and H. C. Greenwell, *Ion adsorption at clay-mineral surfaces: the hofmeister series for hydrated smectite minerals,* Clays and Clay Minerals **64**, 472 (2016).

[65] I. S. Joung and T. E. Cheatham III, *Molecular dynamics simulations of the dynamic and energetic properties of alkali and halide ions using water-model-specific ion parameters,* The Journal of Physical Chemistry B **113**, 13279 (2009).

A

Force Field Parameters

The parameters (ϵ, σ, mass and charge) used to calculate the interatomic potentials are stored in a forcefield. This thesis uses the Interface Force Field (IFF) for silica [58] and Madrid-2019 for the ions [59], which also includes the TIP4P/2005 water model.

Table A.1: The mass and charges of all atom types in the simulation.

Name	**Description**	**Masses (gr/mole)**	**Charges (e)**
Ow	Water oxygen	15.999	-1.1128
Hw	Water hydrogen	1.008	0.5564
Ob	Bridge oxygen, O attached to only Si	15.999	-0.55
Sib	Bridge silicon, Si attached only to Ob	28.085	1.1
Od	Dangling oxygen, O in >SiO^-	15.999	-0.75
Sid	Dangling silicon, Si in >SiO^-	28.085	0.725
Sidd	Double dangling silicon, Si in geminal >SiO^-	28.085	0.35
Os	Silanol oxygen, O in >SiOH	15.999	-0.675
Sis	Silanol silicon, Si in >SiOH	28.085	1.1
Siss	Double silanol silicon, Si in geminal >SiOH	28.085	1.1
Hs	Silanol hydrogen, H in >SiOH	1.008	0.4
Na	Sodium ion	22.99	0.85
Cl	Chloride ion	35.45	-0.85
Ca	Calcium ion	40.078	1.7

Table A.2: The bond coefficients of all bonded atoms in the simulations.

Bond coefficients K_1 (kcal/mole/Å^2)	
OwHw	0.9572
SiO	1.68
OH	0.945

Table A.3: The angle coefficients K_2 between certain atoms in the simulations.

Angle coefficients K (kcal/mole)	
HwOwHw	104.52
SiOSi	149
OSiO	109.5
SiOH	115

Table A.4: LJ-parameter σ_{ij} between all atoms in the simulations.

σ_{ij} (Å)	Ow	Hw	Ob	Sib	Od	Sid	Sidd	Os	Sis	Siss	Hs	Na	Cl	Ca
Ow	3.1589	2.07945	3.12515	3.42805	3.12515	3.42805	3.42805	3.12515	3.42805	3.42805	2.06275	2.60838	4.23867	2.4
Hw		1	2.0457	2.3486	2.0457	2.3486	2.3486	2.0457	2.3486	2.3486	0.9833	1.608685	2.84953	1.8328
Ob			3.0914	3.3943	3.0914	3.3943	3.3943	3.0914	3.3943	3.3943	2.029	2.575631	4.20226	2.422818
Sib				3.6972	3.3943	3.6972	3.6972	3.3943	3.6972	3.6972	2.3319	2.957285	4.19813	3.1814
Od					3.0914	3.3943	3.3943	3.0914	3.3943	3.3943	2.029	2.575631	4.20226	2.422818
Sid						3.6972	3.6972	3.3943	3.6972	3.6972	2.3319	2.957285	4.19813	3.1814
Sidd							3.6972	3.3943	3.6972	3.6972	2.3319	2.957285	4.19813	3.1814
Os								3.0914	3.3943	3.3943	2.029	2.575631	4.20226	2.422818
Sis									3.6972	3.6972	2.3319	2.957285	4.19813	3.1814
Siss										3.6972	2.3319	2.957285	4.19813	3.1814
Hs											0.9666	1.591985	2.83283	1.8161
Na												2.21737	3.00512	2.441485
Cl													4.69906	3.15
Ca														2.6656

Table A.5: LJ-parameter ϵ_{ij} between all atoms in the simulations.

ϵ_{ij} (kcal/mol)	Ow	Hw	Ob	Sib	Od	Sid	Sidd	Os	Sis	Siss	Hs	Na	Cl	Ca
Ow	0.185207	0	0.100006	0.131241	0.150317	0.131241	0.131241	0.150317	0.131241	0.131241	0.052708	0.189624	0.014814	1.732792
Hw		0	0	0	0	0	0	0	0	0	0	0	0	0
Ob			0.054	0.070866	0.081166	0.070866	0.070866	0.081166	0.070866	0.070866	0.02846	0.102391	0.007999	0.850177
Sib				0.093	0.106518	0.093	0.093	0.106518	0.093	0.093	0.03735	0.180906	0.04135	0.106178
Od					0.122	0.106518	0.106518	0.122	0.106518	0.106518	0.042778	0.153902	0.012024	1.277887
Sid						0.093	0.093	0.106518	0.093	0.093	0.03735	0.180906	0.04135	0.106178
Sidd							0.093	0.106518	0.093	0.093	0.03735	0.180906	0.04135	0.106178
Os								0.122	0.106518	0.106518	0.042778	0.153902	0.012024	1.277887
Sis									0.093	0.093	0.03735	0.180906	0.04135	0.106178
Siss										0.093	0.03735	0.180906	0.04135	0.106178
Hs											0.015	0.072653	0.016606	0.042642
Na												0.351902	0.343904	0.20654
Cl													0.018385	0.239006
Ca														0.121224

B

Other Structural Properties

B.1. Total Charge and Ion Density

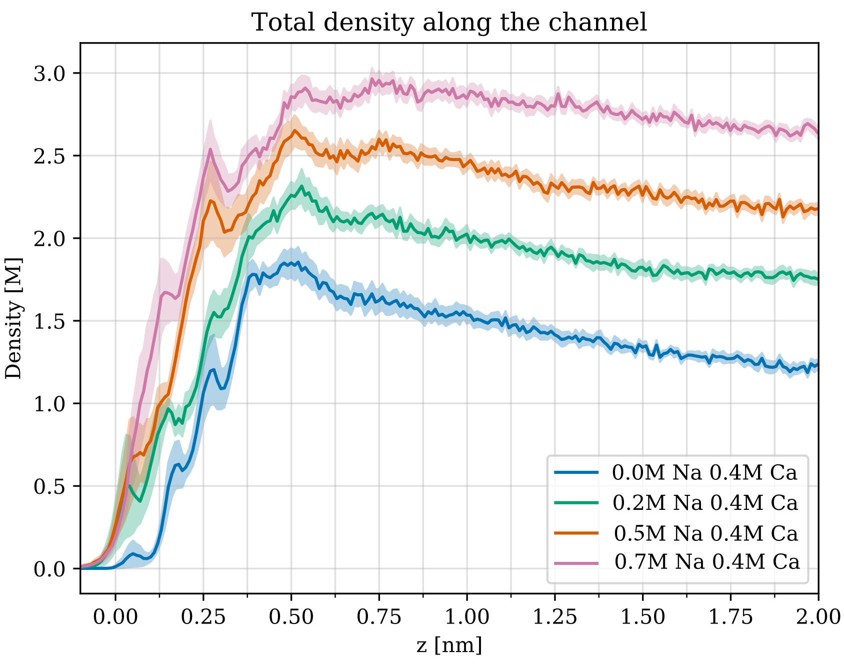

Figure B.1: The total density of all ions for each concentration.

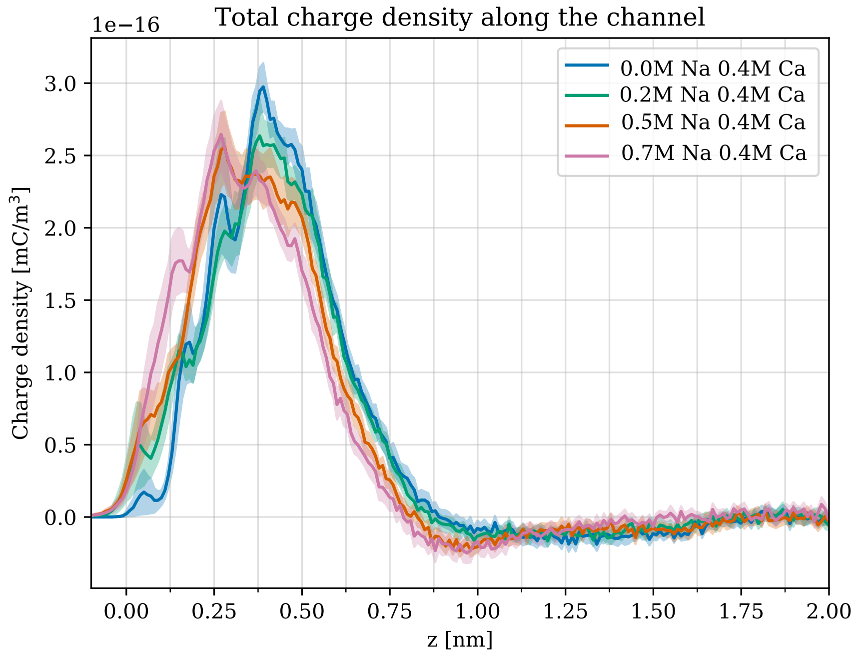

Figure B.2: The total charge density of all ions for each concentration.

B.2. Ion Pairing

The ion pairing was determined by analysing the average distance between cations and anions. The classification of ion pairs is shown in table B.1. These values were determined from the radial distribution function between cations and anions. The distance from the cation of an ion pair to the closest wall atom is plotted.

Note that the ion pairing density is not normalized to the ion density in the channel. Still, it is visbile that no obvious pairing is present in the EDL. Sodium seems to form more pairs with chloride than calcium in the bulk if we look at the orange line for 0.5 M NaCl and 0.4 $CaCl_2$. It is unknown why this is the case.

Table B.1: Ion pair type determination

Ion pair type	**Distance** [Å]
Contact ion pair (CIP)	<3.5
Solvent separated ion pair (SIP)	<5.75
Two solvent separated ion pair (SSIP)	<8

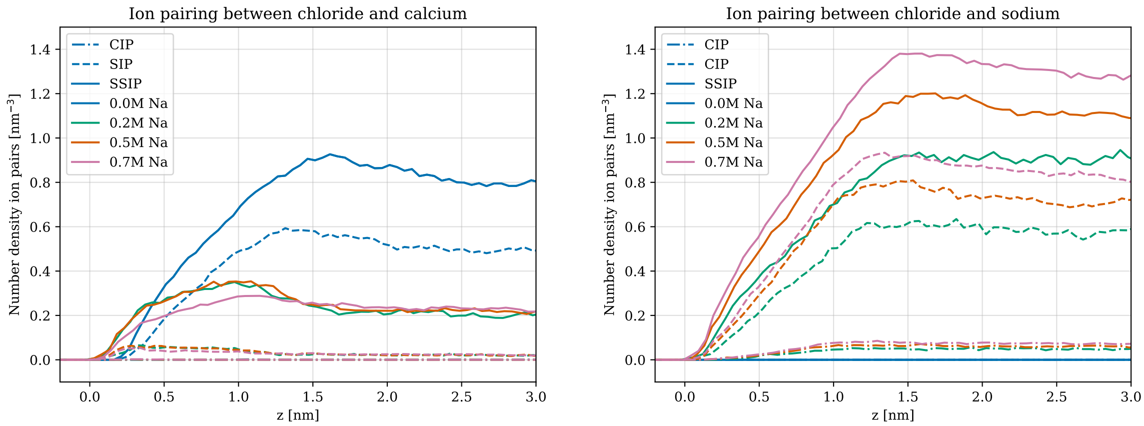

(a) Pairing between calcium and chloride.

(b) Pairing between sodium and chloride.

Figure B.3: Pairing of calcium and sodium with chloride along z.

B.3. Screening Contribution per Type

It can be seen that the ISSC contribution to screening of the bare surface charge increases with increasing NaCl concentration, while the OSSC contribution decreases.

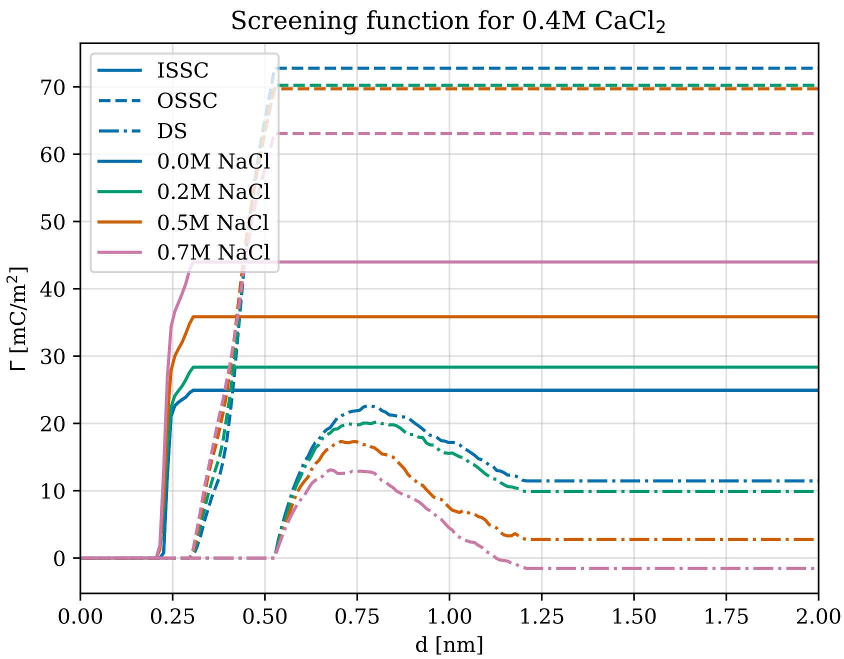

Figure B.4: The screening per adsorption type.

C

Other Electrokinetic Properties over Time

C.1. Velocity over Time

The value used for average EOF is at the cumulative velocity at 70 nanoseconds. The graphs show that the average over the last 25 nanoseconds is representative.

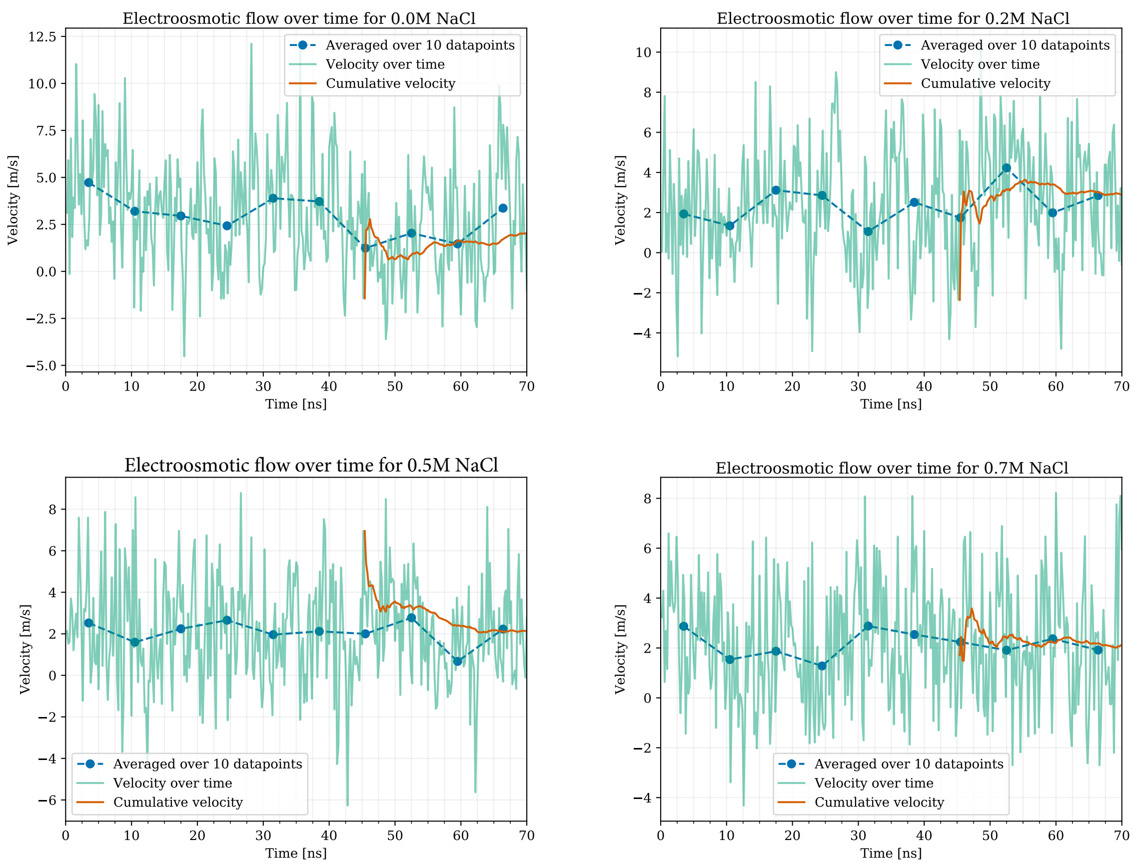

Figure C.1: Velocity profiles over 70 ns for each concentration.

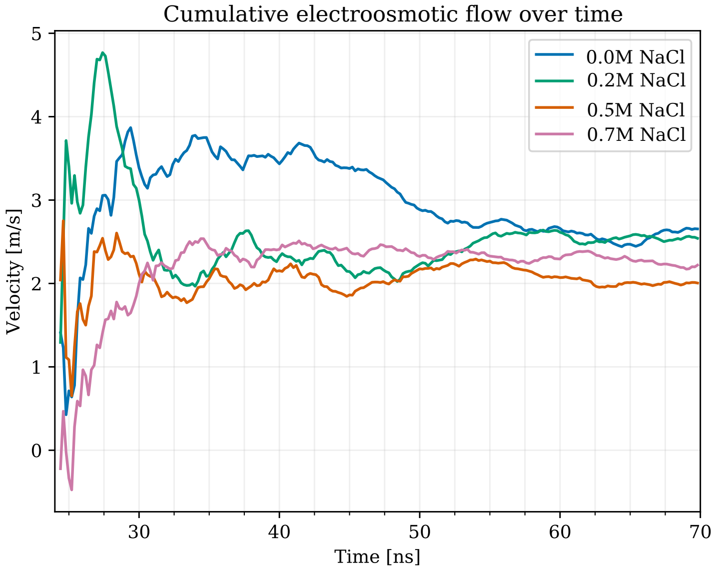

Figure C.2: The cumulative average over the last 25 ns.

C.2. Adsorption against Velocity over Time Time

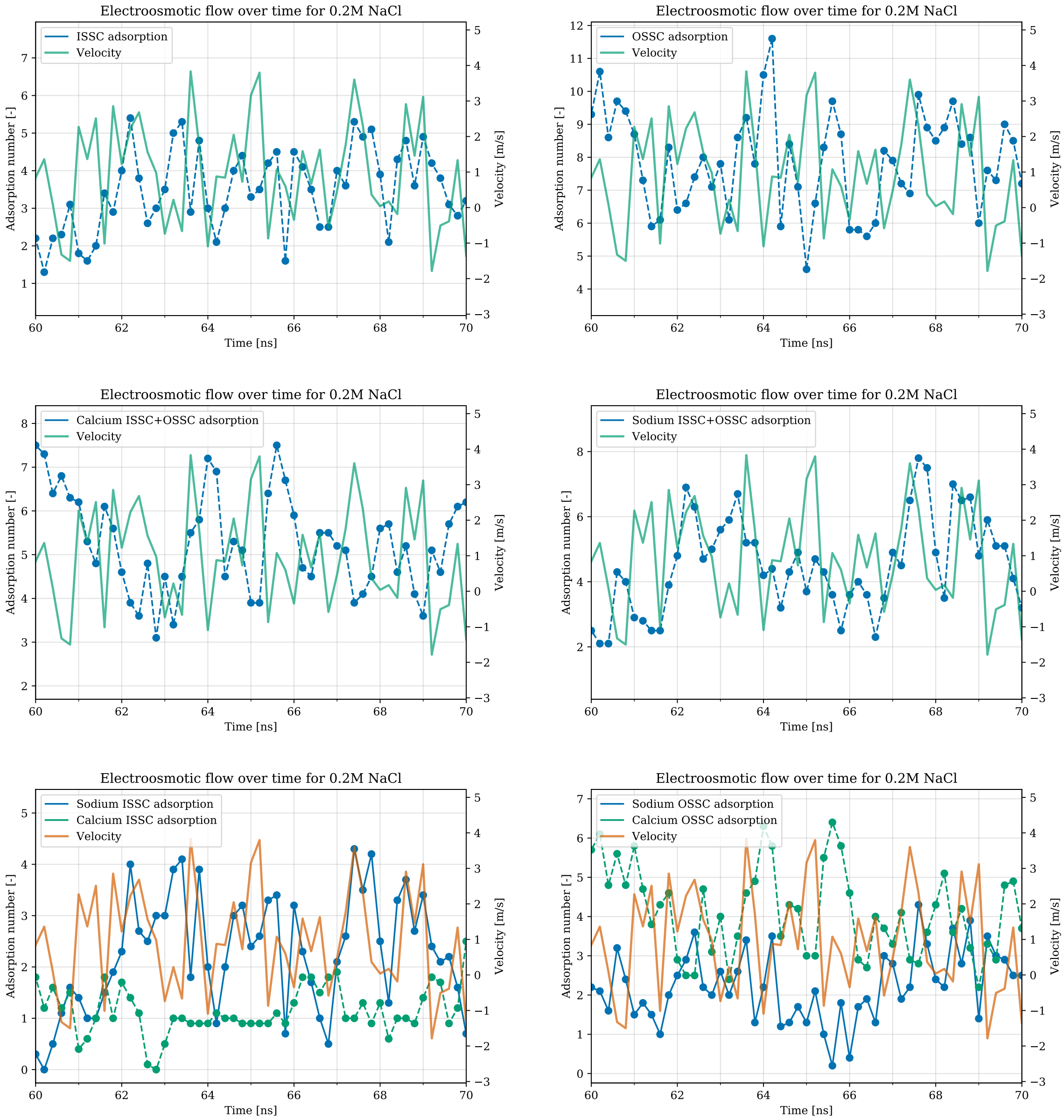

Figure C.3: Adsorption against electroosmotic flow for 0.2M NaCl.

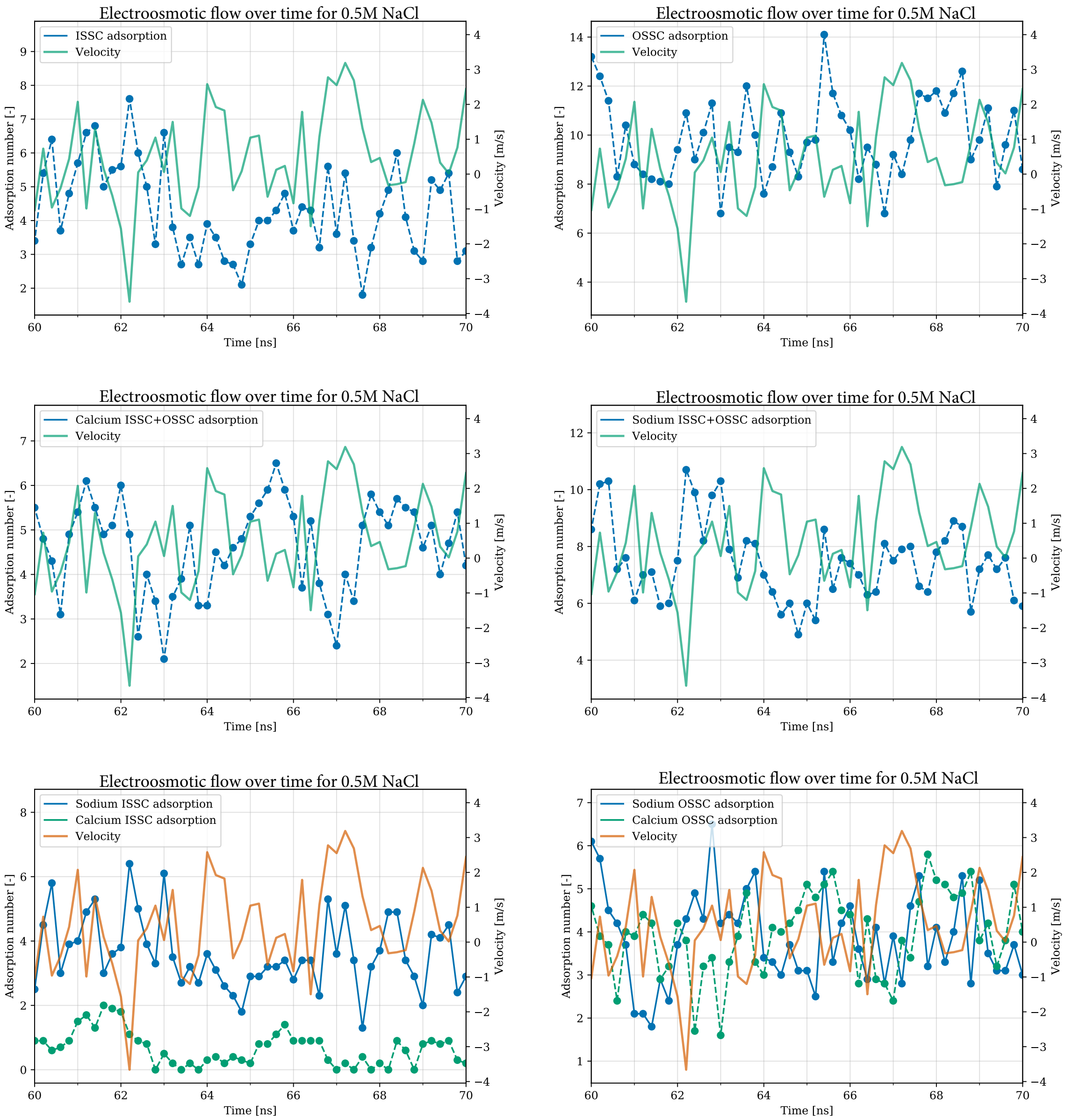

Figure C.4: Adsorption against electroosmotic flow for 0.4M NaCl.

D
Determination of the Shear Plane Location

The intersection between the electric potential and the zeta potential is defined as the theoretical shear plane location. The error of the theoretical shear plane location is determined by the intersection between the error margin of the zeta potential and the electric potential.

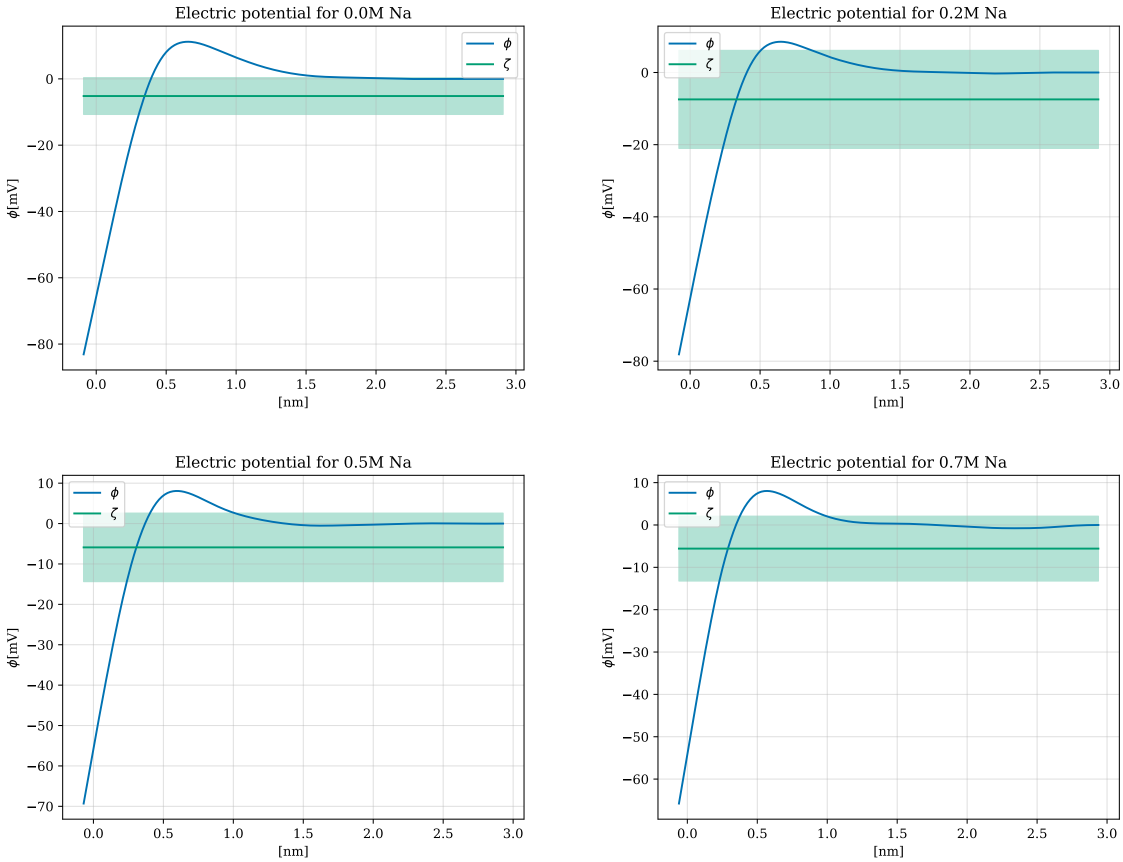

Figure D.1: Electric potential against zeta potential.